



Going with the flow — Changes of vorticity control gold enrichment in Archean shear zones (Shebandowan Greenstone Belt, Superior Province, Canada)

Tobias Stephan ^a*, Noah J. Phillips ^a, Hanna Tiiotto ^a, Adrian Perez ^a, Michael Nwakanma ^a, Robert Creaser ^b, Pete Hollings ^a

^a Department of Geology, Lakehead University, Thunder Bay, ON, Canada

^b Department of Earth & Atmospheric Sciences, University of Alberta, Edmonton, AB, Canada

ARTICLE INFO

Dataset link: [10.17605/OSF.IO/C4EY9](https://doi.org/10.17605/OSF.IO/C4EY9)

Keywords:

Vorticity
Gold
EBSD
TIMS geochronology
Circular kriging
Cyclic fault-valve

ABSTRACT

Archean orogenic gold deposits are commonly hosted in brittle-ductile shear zones, where gold is locally remobilized and reprecipitated due to changes in physio-chemical conditions. However, in Archean rocks of the Superior Craton, these shear zones are often sparsely exposed and inferred primarily through spatial correlation, hence these shear zone architectures remain poorly understood. Here, we apply geochronology, kinematic analysis, and vorticity analysis techniques to study the Shebandowan Greenstone Belt in Northern Ontario, Canada. Geochronological results from zircon U-Pb CA-ID-TIMS and molybdenite Re-Os NTIMS dating yielded an age of 2717.35 ± 0.48 Ma for a proximal felsic intrusion and 2708 ± 12 Ma for auriferous and molybdenite-bearing vein mineralization, respectively. Field observations and regional age data indicate that both mineralization and intrusive activity predate deformation. Spatial interpolation of ductile foliation orientations reveals that gold mineralization is spatially associated with abrupt changes in shear zone orientation. Vorticity analysis — including rigid porphyroblast and crystallographic vorticity analysis — shows that these changes induce strain partitioning in releasing and restraining bends. These observed localized deflections in shear zone strike are attributed to the competency contrast between the old, feldspar-rich, isotropic, and syenitic plutonic bodies (rheologically stronger) and gold-bearing, intermediate metavolcanic and diorite units (rheologically weaker). Transitions from non-coaxial to coaxial flow dominated areas appear to have localized fluid pathways, allowing for fluid migration and gold precipitation during deformation. Quantifying deflections of shear zones adjacent to rigid geological bodies, combined with analyzing the deformation flow types, represents a powerful and cost-effective tool for gold exploration in granite-greenstone belts.

1. Introduction

The majority of worldwide gold deposits formed in Archean greenstone belts (Frimmel, 2008; Goldfarb et al., 2005; Sillitoe, 2020) highlighting that Archean tectonics was highly effective at transferring gold from the mantle and concentrating it locally in the lithosphere (Frimmel, 2008; Goldfarb and Groves, 2015; Romer and Kroner, 2018; Goldfarb et al., 2005; Phillips and Powell, 2009; Sillitoe, 2020; Goldfarb and Pitcairn, 2023). Most Archean gold occurs in structurally hosted lode gold systems within metamorphic terranes linked to accretionary and collisional orogens (Kerrick and Cassidy, 1994; Kerrich and Wyman, 1990; Groves et al., 1998; Campbell McCuaig and Kerrich, 1998). Orogenic gold is generally thought to derive from aqueous-carbonaceous fluids released during partial melting or prograde metamorphism of

Archean basement rocks (Goldfarb et al., 2005; Phillips and Powell, 2009; Sillitoe, 2020; Goldfarb and Pitcairn, 2023; Wood et al., 1986; Burrows and Spooner, 1987; Duuring et al., 2007; Kerrich and Cassidy, 1994; Pitcairn et al., 2006). However, the low solubility of gold implies that enormous volumes of fluids are required to produce deposit-scale concentrations of 1 to locally $> 100,000$ ppm (Rauchenstein-Martinek et al., 2014; Williams-Jones et al., 2009). Hence, localized secondary processes must play a major role in further concentrating gold. Gold is typically remobilized by sulfide dissolution-reprecipitation (Hastie et al., 2020; Fougerouse et al., 2016) or dynamic recrystallization (Dusbosc et al., 2018), and subsequently transported in solution (Seward, 1973; Seward et al., 2014; Shenberger and Barnes, 1989; Kolb, 2008;

* Corresponding author.

E-mail address: tstephan@lakeheadu.ca (T. Stephan).

Williams-Jones et al., 2009), in low-temperature Bi-Te melts (Melo-Gómez et al., 2025; Hastie et al., 2020, 2021; Tomkins et al., 2004, 2007; Frost et al., 2002; Tooth et al., 2011), or as colloids (e.g. Petrella et al., 2020; McNab et al., 2024; Hastie et al., 2021; Voisey et al., 2020). The vast majority of gold-bearing veins are hosted in purely ductile shear zones or brittle-ductile faults (e.g. Hodgson, 1989; Sillitoe, 2020; Goldfarb et al., 2005; Blenkinsop et al., 2020), where episodic fracturing and fluid flow facilitates gold precipitation (i.e., the “fault-valve model”; Sibson et al., 1975, 1988; Cox et al., 1995; Cox, 2016; Weatherley and Henley, 2013; Yardley, 1996; Gold and Soter, 1984). Structural features that enhance permeability or trap fluids include fault intersections, fold hinges, and restraining or releasing bends — also known as dilatational or contractional jogs ductile shear zones or brittle ductile faults (e.g. Blenkinsop et al., 2020; Newhouse, 1942; Hodgson, 1989; Cox et al., 1991; McKinstry, 1948; Micklethwaite and Cox, 2006).

Recognizing zones of dilation or contraction at the regional scale can be as challenging as locating the deposits themselves. Locating such features often requires substantial rock exposure or extensive drilling, both of which are limited in glacially eroded and heavily vegetated regions such as the Canadian Shield. Because dilatational and contractional jogs imply bending and changes of the kinematics of the foliation, these relationships provide an opportunity to locate these zones indirectly, even when rock exposure is limited. Whether zones of permeable pathways form around specific structures (e.g., rigid rock bodies) ultimately depends on the strain geometry and kinematics — features that are not always evident from interpolations of regional fabrics in regions of poor exposure.

In this contribution, we use the Archean Shebandowan Greenstone Belt to test whether gold is spatially correlated with specific strain geometries and kinematics (Fig. 1). We integrate geochronology, spatial analysis of the regional foliation, and vorticity estimates derived from both rigidly rotated porphyroclasts and intragranular distortions. The combination of these methods reveals that undeformed granitoid bodies predate the gold-bearing shear zones and hence, acted as rigid obstacles during ductile deformation, particularly within a zone with a high contribution of simple shear. We propose that deflections of the foliation within the zone of elevated simple shear caused strain partitioning and localized permeability, ultimately leading to concentration of gold.

2. Geological background

The gold deposits of the Shebandowan Greenstone Belt are located within the Wawa-Abitibi Subprovince of the Superior Craton, along its northern boundary to the metasedimentary assemblages of the Quetico Subprovince (Percival et al., 2012). The belt comprises Neoarchean volcano-sedimentary sequences metamorphosed from greenschist to upper amphibolite grades (Corfu and Stott, 1986, 1998; Corfu, 2000; Hart, 2007; Ayer et al., 2002, 2005; Thurston et al., 2008). Based on geochronology, the belt is subdivided into three assemblages, the ca. 2720 Ma Greenwater assemblage, the 2695 Ma Kashabowie assemblage, and the youngest (2682 Ma) metasedimentary Auto Road assemblage (Williams et al., 1991; Corfu and Stott, 1998; Osmani, 1993). The study area in the western Shebandowan Greenstone Belt comprises the Greenwater and Kashabowie assemblages.

The protoliths of the Greenwater assemblage are predominantly tholeiitic basalt with minor komatiitic basalt, komatiitic flows, felsic volcanic flows and pyroclastic units (Carter, 1984; Rogers and Berger, 1994; Osmani, 1997; Corfu and Stott, 1998). U-Pb dating of zircons from the extrusive and intrusive rocks of the Greenwater assemblage yields ages of 2718 to 2722 Ma (Corfu and Stott, 1998). The Kashabowie assemblage is predominantly composed of debris-flow deposits (so-called Timiskaming-type assemblage), sourced from calc-alkalic to alkalic, mafic to felsic volcanic protoliths and clastic metasedimentary rocks (Lodge et al., 2013). This assemblage

appears to be tectonically interleaved with the Greenwater assemblage and has yielded U-Pb zircon ages of 2694 to 2696 Ma (Corfu and Stott, 1998). The main ductile deformation caused subhorizontal stretching and dextral shearing along NE-SW striking foliation, defined by the alignment of metamorphic minerals, such as actinolite, biotite, feldspar, and quartz in the volcanic protoliths and their plutonic equivalents. An older increment of deformation has been suggested based on the locally, steeper (almost vertical) stretching lineation and crenulation (Osmani, 1993). The youngest phase of felsic magmatism at 2670–2650 Ma is interpreted to postdate the ductile deformation (Heather and Shore, 1999; Davis et al., 2000).

The Quetico Subprovince (to the north of the Shebandowan Greenstone Belt) is an ENE-WSW trending belt comprised of metasedimentary rocks (Fig. 1). The unit is mainly composed of metagreywackes and associated paragneisses, migmatites, and peraluminous granite assemblages (Percival, 1989; Percival and Williams, 1989). Deposition of the sedimentary successions is bracketed between 2700 Ma and 2690 Ma (Zaleski et al., 1999; Fralick and Pufahl, 2006; Davis et al., 1990). Detrital zircon age spectra indicate that the sediments were sourced from northerly located subprovinces (Davis et al., 1990; Fralick and Pufahl, 2006; Fralick and Kronberg, 1997). The metamorphic gradient increases from greenschist facies conditions at the Quetico-Wawa subprovince boundary, up to granulite facies conditions (including partial melting) towards the center of the Quetico Subprovince (Pan et al., 1994, 1998; Sawyer, 1983; Sawyer and Barnes, 1988; Borradaile and Spark, 1991). The age of peak metamorphism is bracketed between 2671 and 2665 Ma (Pan et al., 1998). The Quetico Subprovince was affected by folding under NW-SE shortening and perpendicular horizontal stretching (Sawyer, 1983). Fold-cleavage relationships, in particular the existence of a transecting cleavage (oblique to fold-axis planar surface) (Borradaile, 1978) indicates that the deformation occurred under transpression resulting in a flattening strain geometry (Borradaile and Spark, 1991; Borradaile and Schwerdtner, 1984).

2.1. Gold deposits of the Shebandowan Greenstone belt

The Shebandowan Greenstone Belt hosts two past producing gold mines. The “Huronian Mine” (Fig. 1) was discovered in 1870, and operated intermittently between 1882 and 1937, producing approximately 29 629 oz of gold in the latest phase of mining from 1932 through 1936 (Schneiders and Dutta, 1985). Mineralization was associated with NE-trending, sulphide- and telluride-bearing quartz veins cutting schistose, predominantly mafic metavolcanic rocks, locally accompanied by highly altered and mineralized feldspar porphyry. The “North Coldstream Cu-Au-Ag deposit” (Fig. 1) produced 31 493 699 oz of copper, 6 224 oz of gold and 139 505 oz of silver (Giblin, 1964). The easterly plunging (50°) ore-bodies are hosted by siliceous, brecciated chert and occur either as massive sulfide bodies, disseminated sulfide, or as some stringers. Sulfides are predominantly chalcopyrite and pyrite with minor pyrrhotite (Giblin, 1964).

Gold mineralization in the “Moss Deposit” and “East Coldstream Deposit” occur in sheared intermediate to felsic metavolcanic rocks and in sheared and fractured diorite to gabbro or feldspar and quartz-feldspar porphyry bodies emplaced within intermediate to felsic metavolcanic rocks. Mineralization occurs as disseminated sulfides, quartz-albite veining and flooding with alteration minerals consisting mainly of silica, albite, sericite, carbonates, pyrite and minor chalcopyrite (Dufresne and Black, 2024). The deposit has an indicated resource of 1.535 Moz at 1.23 g/t Au and inferred resource estimate of 5.198 Moz contained gold at 1.11 g/t Au (Dufresne and Black, 2024). All three deposits and past producing mines occur within a linear trend along the Quetico-Wawa boundary. Here we test whether there are changes in regional kinematics between the mineralized zone and surrounding unmineralized units.

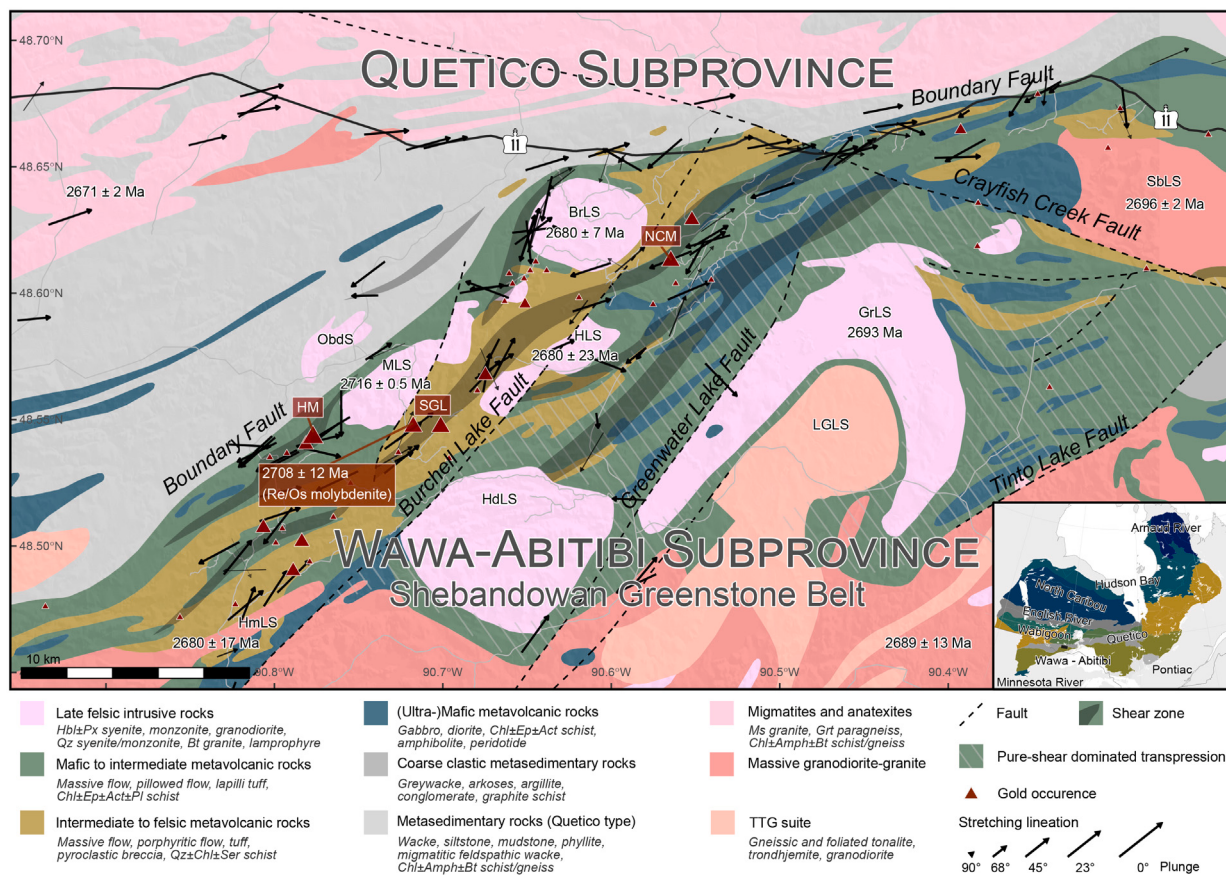


Fig. 1. Geological map of the western Shebandowan Greenstone Belt (modified from Ontario Geological Survey, 2011). Red triangles show known gold occurrences (small triangles), gold prospects (medium), and past gold mines (large) (Ontario Geological Survey, 2024). Inset shows subprovinces of the Superior Craton (modified from Frieman et al., 2017). Abbreviations: BrLS — Burchell Lake Stock, GrLS — Greenwater Lake Stock, HdLS — Hood Lake Stock, HLS — Hermia Lake Stock, HM — Huronian Mine, HmLS — Hamlin Lake Stock, LGLS — Little Greenwater Lake Stock, MLS — Moss Lake Stock, NCM — North Coldstream Mine, ObdS — Obadinaw Stock, SbLS — Shebandowan Lake Stock, SGL — Snodgrass Lake deposit. Ages are compiled from various sources (see Tab. S2).

3. Methods

3.1. Orientation analysis

Regional field mapping was done to determine the orientations of the foliation and stretching lineation as well as the kinematics of deformation. The structural data and field notes are available through the StraboSpot project repository in Stephan (2025).

To show statistical variations of orientation data in terms of their three-dimensional distribution (clustered, girdle or random), we visualize the foliation and lineation data of the different grouped outcrops on a “fabric plot” after Vollmer (1990). The diagram displays the ratio of the three eigenvalues (ϵ_1 , ϵ_2 , and ϵ_3) corresponding to the three eigenvectors of the orientation matrix that represents the distribution of the foliation and lineation data (Scheidegger, 1964; Lisle, 1989; Woodcock, 1977). These eigenvalues allow quantification of the shape of the distribution, which can be a combination of a point (clustered), girdle, and random shape (Vollmer, 1990). For this analysis, the outcrops were grouped regionally based on proximity and similar orientations.

Based on the test statistic of the uniformity test against the alternative hypothesis of a Bingham distribution (Mardia and Jupp, 2000), a linearized measure for uniformity is given by

$$U = 1 - \sqrt{\frac{3}{2}} \sum_{i=1}^3 \left(\epsilon_i - \frac{1}{3} \right)^2 \quad (1)$$

$U \in [0, 1]$ represents the uniformity, i.e. a spherical uniform distribution yields $U = 0$, a Bingham distribution (i.e. “girdle”) is $U = 0.5$, and a von Mises–Fisher distribution (i.e. “cluster”) is $U = 1$ Lisle

(1985), Vollmer (2020). The 95% confidence interval for the uniformity index for each outcrop group is estimated from 1000 bootstrap samples.

The spatial trend of the strike of the foliation at surface can be spatially interpolated using the strike data. We perform a Krige interpolation algorithm for circular data based on the R package Circ-Spatial (Morphet and Symanzik, 2010) using the average orientation of the foliation in each outcrop. Because perturbations of the foliation orientation result in a high local variance of the foliation strike, we map these deflections by applying an adaptive kernel window to measure the circular variance of the foliation strike within the kernels, weighted by the inverse of the distance to neighboring data points. The algorithm is based on the R package tectonicr (v0.4.1.9) (Stephan et al., 2023; Stephan, 2024).

3.2. Vorticity analysis

3.2.1. Rigid porphyroblast rotation

The mean kinematic vorticity number W_m (Means et al., 1980; Truesdell, 1953) describes the bulk rotation of material lines coincident with the principal strain axes and ranges between 0 for pure shear strain and 1 for simple shear strain. The vorticity number is given as $W_m = \cos \alpha$ with α being the angle between the flow apophyses, which bisect flow fields of forward and backward rotation with respect to the shear direction. An equal contribution to strain from both pure shear (flow apophyses are perpendicular, i.e. $\alpha = 90^\circ$) and simple shear components (parallel apophyses, i.e. $\alpha = 0^\circ$) occurs at $\alpha = 45^\circ$, and hence, $W_m = 0.71$ (Law et al., 2004).

The rotation of rigid porphyroclasts embedded in a ductilely deforming matrix depends on the vorticity of flow (Passchier, 1987; Simpson and De Paor, 1993; Xypolias, 2010). Thus, the relationship of the aspect ratio of a porphyroblast and its orientation with respect to the tectonic foliation can be used to estimate a mean kinematic vorticity number, W_m (Ghosh and Ramberg, 1976; Jessup et al., 2007; Larson and Godin, 2009; Law et al., 2004; Passchier, 1987; Simpson and De Paor, 1993). We use the rigid grain net (RGN) method of estimating W_m (Jessup et al., 2007). The RGN relates the aspect ratio and long axis orientation of tailless porphyroclasts to W_m (Fig. 5). Specimens must therefore meet the following criteria: (1) the porphyroclasts have undergone no internal deformation; (2) the matrix surrounding the clast was homogeneously deformed; (3) sufficient strain has developed to allow all clasts to reach a stable sink position; and (4) there has been no mechanical interaction between rigid porphyroclasts (Jessup et al., 2007; Simpson and De Paor, 1993; Simpson and De Paor, 1997). Microscopic inspection of thin sections cut from porphyroblast-bearing specimens collected during this study indicates that only 13 such specimens appear to meet all the criteria necessary for vorticity analysis by the RGN method (sample locations and descriptions in Tab. S1). Although rigid porphyroblast rotation-based determinations of W_m assume a minimum of monoclinic symmetry, they do not assume plane-strain deformation and remain valid for three-dimensional strains (Law et al., 2004). The true value for W_m can only be observed in a plane parallel to both the vorticity axis and the foliation. Thus, we determine W_m from thin sections that — if not stated otherwise — are cut parallel to the mean stretching lineation (X) and perpendicular to the foliation (Z) while assuming monoclinic shear, where the vorticity profile plane (VPP) coincides with the XZ plane. It is worth noting that the assumption of monoclinic shear deformation is commonly not satisfied (as shown by the crystallographic vorticity analysis). Hence all W_m analyses from the XZ plane of the finite strain ellipsoid underestimate the bulk rock's vorticity.

We digitized the aspect ratio (R , i.e. ratio of the clast's long axis and short axis) and the angle between the foliation and the long axis (ψ , measured clockwise for positive angles) of the porphyroclasts clasts from scanned thin-sections using the software *EllipseFit* 3.11.0 (F. Vollmer: <https://www.frederickvollmer.com/ellipsefit/index.html>). The angle ϕ is the difference between the measured orientation of the clasts' long axes with respect to an arbitrary line and the circular mean of these orientations (weighted by the clasts' aspect ratio), because the mean long-axis orientation represents a best-fit of the foliation's orientation. Scans and measurements are documented in the file *S3_vorticity.zip* in the supplementary material.

The boundary between freely spinning (infinitely rotating) porphyroclasts and those that have entered a “stable sink” position (limited rotation) is given by the grain with the maximum shape factor and an orientation larger than the critical angle (Passchier, 1987)

$$\psi_c = \frac{1}{2} \sin^{-1} \frac{W_m}{B_c} \left(\sqrt{1 - W_m^2} - \sqrt{B_c^2 - W_m^2} \right) \quad (2)$$

with the shape factor

$$B_c = \frac{R^2 - 1}{R^2 + 1}. \quad (3)$$

Thus, the maximum shape factor of the freely spinning grains is an estimate for the mean kinematic vorticity number W_m (Jessup et al., 2007). Here we use 97.5% upper quantile instead of the maximum B_c to avoid outliers. There is a potential error introduced by slightly oblique cuts of the rock specimens and thin section, as well as slight changes in orientation due to wavy foliation, so we discard clasts that are only 3° larger than the critical orientation. The 95% confidence interval for the critical shape factor B_c for each specimen is estimated from 10 000 bootstrap samples.

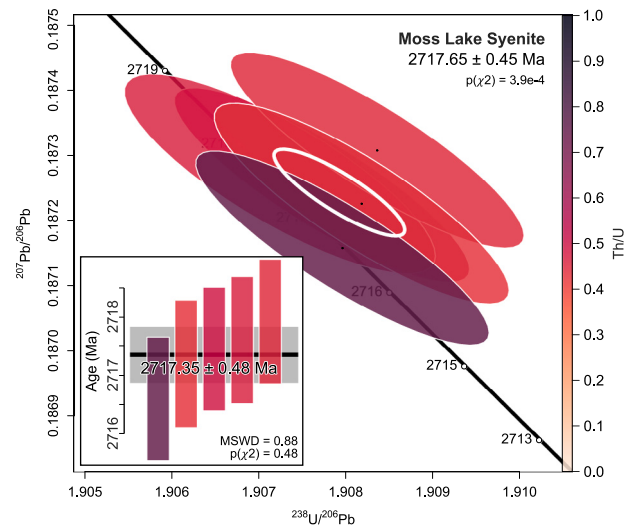


Fig. 2. CA-ID-TIMS results of zircon U-Pb dating of Moss Lake Syenite Stock (Fig. 1). (A) Tera–Wasserburg concordia diagram showing the isotopic ratio measurements as 2σ analytical uncertainty ellipses, the concordia age (white ellipse), and the p -value of the χ^2 test for goodness-of-fit. Inset shows the weighted mean age of the single grain ages with their 2σ uncertainties (including mean square weighted deviation (MSWD) and p -value of the χ^2 test). Grey area shows the 2σ error of the calculated weighted mean age. Isotope ellipses and age bars of individual zircons are colored by their Th/U ratios.

3.2.2. Crystallographic vorticity axes

The position of the rock's bulk vorticity vector with respect to the maximum stretching direction allows characterization of the flow regime for steady-state deformation. In the strain reference system (where X, Y and Z characterize the maximum stretching, intermediate strain and maximum shortening directions, respectively) a monoclinic pure-shear zone contains a vorticity axis parallel to X, whereas a vorticity axis parallel to Y occurs in a monoclinic simple shear zone. Any other orientation of the vorticity axis with respect to the strain coordinates indicates triclinic shearing. To identify the orientation of the rock's bulk vorticity axis, we use the crystallographic vorticity axis (CVA) that determines the position of grain-scale vorticity axes (i.e. one vorticity axis per grain; Michels et al., 2015). The methodology uses rotational statistics to calculate the position of a rotational axis that matches the intragranular dispersion of crystallographic orientations in a single deformed grain Michels et al. (2015). Crystallographic orientations were collected through electron backscatter diffraction analysis of 10 oriented samples. Analyzed sample surfaces were cut parallel to the macroscopic stretching lineation and perpendicular to the foliation.

Data from 10 samples were acquired at the University of British Columbia Okanagan, using a Tescan Mira 3 XMU variable pressure scanning electron microscope (tungsten filament; 20 kV and 25 Pa conditions) equipped with an Oxford Instruments Symmetry S-3 detector. Sample locations and descriptions are listed in Table S1.

Crystalllographic orientation maps were collected for each sample at step sizes ranging from 1 to 10 μm using a 30 kV acceleration voltage, 20.6 nA beam current, a gain ranging from 1 to 2, Speed 1 mode, frame averaging ranging from 1 to 5, and a 10%–15% overlap between the maps. Grain orientation maps were processed using MTEX v6.0.beta3 (Bachmann et al., 2010; Hielscher and Schaeben, 2008; Schaeben et al., 2007). Grain boundaries were defined using a 10° misorientation threshold and grains with less than 4 orientation solutions were omitted. Quartz grains with a shared neighbor-neighbor misorientation of $60^\circ \pm 1^\circ$ were merged as they represent Dauphiné twin boundaries. We calculate grain-scale CVA using the method described in Michels et al. (2015) for grains that have a grain orientation

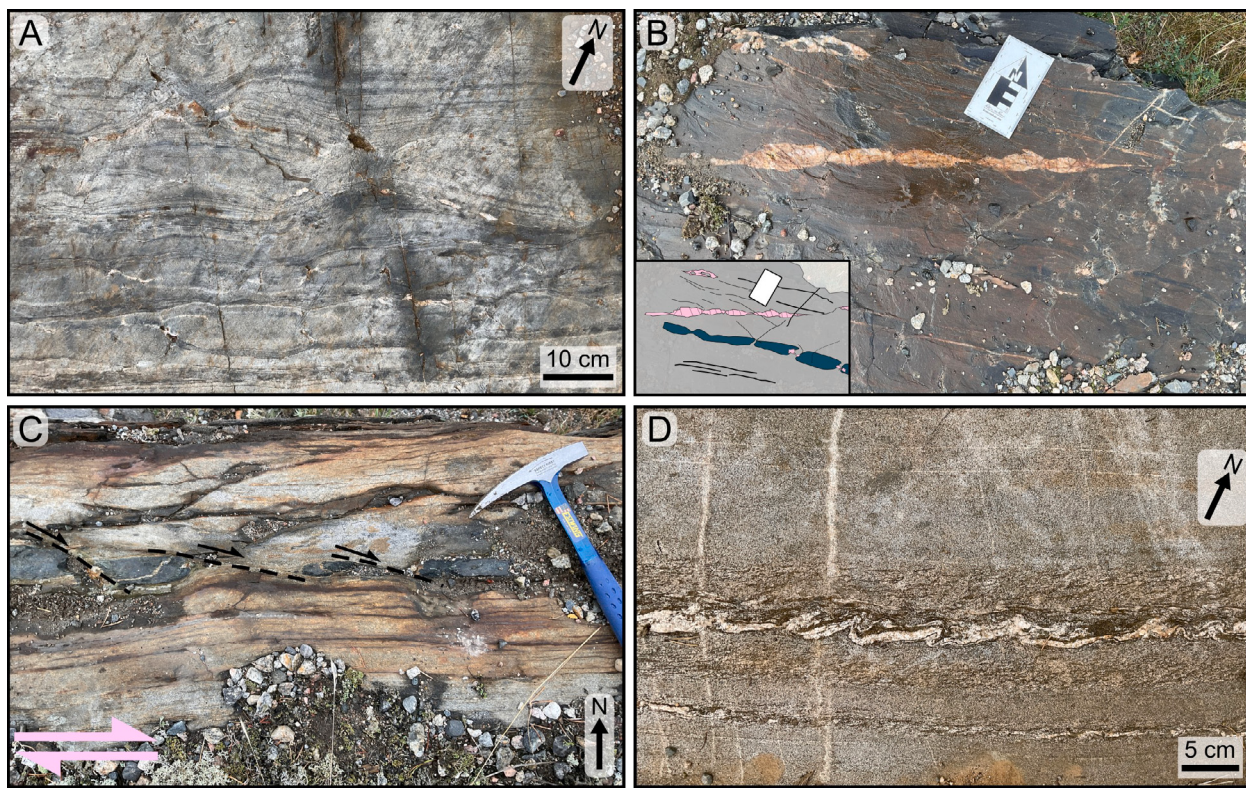


Fig. 3. Field photographs of structures in subhorizontal pavements from the Quetico Subprovince. (A) Fishmouth-type foliation boudinage structures (location: 90.6270°W, 48.6488°N). (B) Dextral shearband boudins and asymmetric foliation boudinage structures (location: 90.6310°W, 48.6515°N). (C) Dextral shearband boudins in Grt-paragneiss. (location: 90.6888°W, 48.6545°N). (D) Migmatitic paragneiss with asymmetric fold indicating dextral sense of shear (location: 90.8271°W, 48.6618°N).

spread larger than 1°. Density functions were constructed using a 7.5° halfwidth de La Vallée Poussin kernel. To extract the orientation of the vorticity axis in geographic coordinates, we rotate the CVAs from the EBSD coordinate system into the geographic coordinate using the thin-section and sample orientation as transformation parameters. In a final step, we estimate the kinematic vorticity number and the amount of triclinic shear using the intersection of the VPP with the foliation and the plane perpendicular to the foliation and lineation, respectively.

3.3. Geochronology

3.3.1. Zircon U-Pb CA-ID-TIMS

Zircon from the Moss Lake Stock (48.551°N, 90.717°W; Fig. 1) were selected for U-Pb geochronology at the Pacific Centre for Isotopic and Geochemical Research (UBC Vancouver).

The syenite sample was first crushed and ground and minerals were separated by water-table (Wilfley table), heavy-liquid and magnetic separation (Frantz magnetic separator). Zircon grains or grain fragments were manually picked under magnification and five crack-and-inclusion free grains were selected for CA-ID-TIMS U-Pb dating (Scoates and Friedman, 2008). For the isotope-dilution analysis, the grains were dissolved and homogenized with the chemical abrasion, single-grain U-Pb technique using an EARTHTIME ET535 tracer to be finally analyzed using a Nu Instruments thermal ionization mass spectrometer. Common Pb correction is applied on our U-Pb data by inferring the initial common Pb composition from the two-stage crustal evolution model of Stacey and Kramers (1975). Isotope and calculated grain ages are listed in the supplementary material. The Tera-Wasserburg concordia diagram is shown in Fig. 2.

3.3.2. Molybdenite Re-Os NTIMS

One molybdenite-bearing sample was selected from an auriferous and shear zone-parallel quartz vein (> 0.24 ppm Au; Goldshore Resources Inc., personal communication, 2023) within a deformed metadiorite (48.546°N 90.705°W; Fig. 1) for Re-Os geochronology obtained at the Canadian Centre for Isotopic Microanalysis (University of Alberta).

Methods used for molybdenite analysis are described in detail by Selby and Creaser (2004). Areas of the sample with visible molybdenite were removed, and preparation of a molybdenite mineral separate was made by metal-free crushing and sieving followed by magnetic and gravity concentration methods. The ^{187}Re and ^{187}Os concentrations in molybdenite were determined by isotope dilution mass spectrometry using Carius-tube, solvent extraction, anion chromatography and negative thermal ionization mass spectrometry (NTIMS) techniques. For this work, a mixed double spike containing known amounts of isotopically enriched ^{185}Re , ^{190}Os , and ^{188}Os analysis was used (Markey et al., 2007). Isotopic analysis used a ThermoScientific Triton mass spectrometer by Faraday collector. Total procedural blanks for Re and Os are less than < 3 pg and 2 pg, respectively, which are insignificant in comparison to the Re and Os concentrations in molybdenite. The Reference Material 8599 Henderson molybdenite (Markey et al., 2007) is routinely analyzed as a standard, and during the past 8 years returned an average Re-Os date of 27.78 ± 0.07 Ma ($n=44$), indistinguishable from the Reference Age Value of 27.66 ± 0.1 Ma (Wise and Watters, 2011). The ^{187}Re decay constant used is $1.666 \cdot 10^{11} \text{ a}^{-1}$ (Smoliar et al., 1996). Additional details are listed in the supplementary material (S2_geochronology.xlsx).

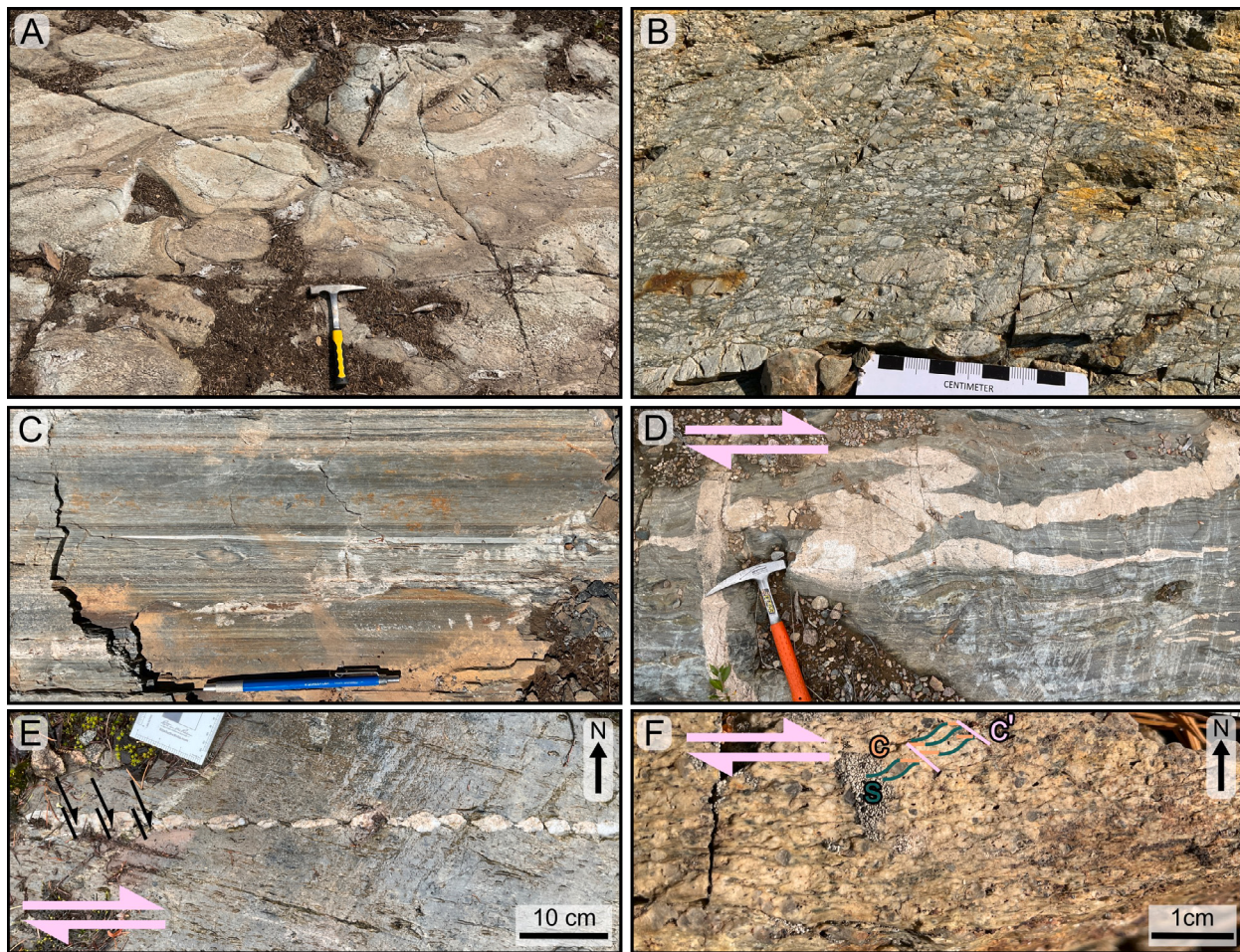


Fig. 4. Field photographs of structures in subhorizontal pavements from the Shebandowan Greenstone Belt. (A) Pillow basalt (location: 90.5390°W, 48.6203°N). (B) Flattened felsic metavolcanic rocks. Flattened lapilli have an aspect ratio of $R_{XZ} = 2.46 \pm 0.2$ (location: 90.4423°W, 48.6462°N). (C) Mylonitic foliation in intermediate metavolcanic rock (90.2557°W, 48.6791°N). (D) Sheared migmatitic metavolcanic rock and felsic dike/veins (location: 90.5771°W, 48.4833°N). (E) Dextral Shearband boudinage of quartz vein in intermediate metavolcanic rock (location: 90.5885°W, 48.6435°N). (F) Dextral sc' fabric in meta-granite (location: 90.7120°W, 48.5426°N).

4. Results

4.1. Structures

4.1.1. Quetico subprovince

In the low-grade units of the metasedimentary rocks in the Quetico Subprovince, shear sense indicators are rare, limited primarily to asymmetric foliation boudinage structures (cf. Arslan et al., 2008) (Fig. 3B) and shear boudins (Fig. 3B) that suggest a dextral sense of shear. Higher grade units provide more pronounced evidence of dextral sense of shear, including SC-fabrics, shear bands, and asymmetric folding within paragneiss and deformed migmatitic units (Fig. 3C and D). The finite strain geometry is characterized by flattening (Fig. S6).

4.1.2. Shebandowan Greenstone belt

In the Shebandowan Greenstone Belt of the Wawa-Abitibi Subprovince, we observe a varying degree of deformation as shown by the strain intensity and spacing of the foliation, which result in partitioning between high and low-strain domains. At the outcrop scale, the foliation has an anastomosing pattern producing weakly deformed microlithons or shear boudins (low-strain zone) surrounded by high-strain zones characterized by foliated and strongly deformed rock

(of the same lithologies as observed in the shear boudins). There is an overall dominance of dextral shear sense indicators close to the boundary with the Quetico Subprovince. However, mixed kinematic indicators (the presence of both dextral and sinistral shear senses) and a local dominance of sinistral shear sense indicators are also prevalent. Based on aspect ratio obtained from elongated pillow basalt, the strain geometry is dominantly flattening with $R_{XZ} = 2.46 \pm 0.2$ Fig. 4B and Fig. S6.

4.1.3. Large igneous bodies and plutons

Rocks surrounding the large felsic plutonic bodies in the Shebandowan Greenstone Belt (see Fig. 1) show no evidence of contact metamorphism. Macroscopically, the felsic plutonic rocks, mainly syenites and quartz-monzonites, appear undeformed and lack metamorphic phase transitions. However, microscopically, quartz grains display evidence of intracrystalline deformation (e.g. undulose extinction) and dynamic recrystallization, such as subgrain rotation and bulging recrystallization along quartz-quartz boundaries (Fig. S7). Feldspar grains, in contrast, do not show evidence for dynamic recrystallization, although they exhibit perthite textures and cross-hatching textures in microcline (Fig. S7).

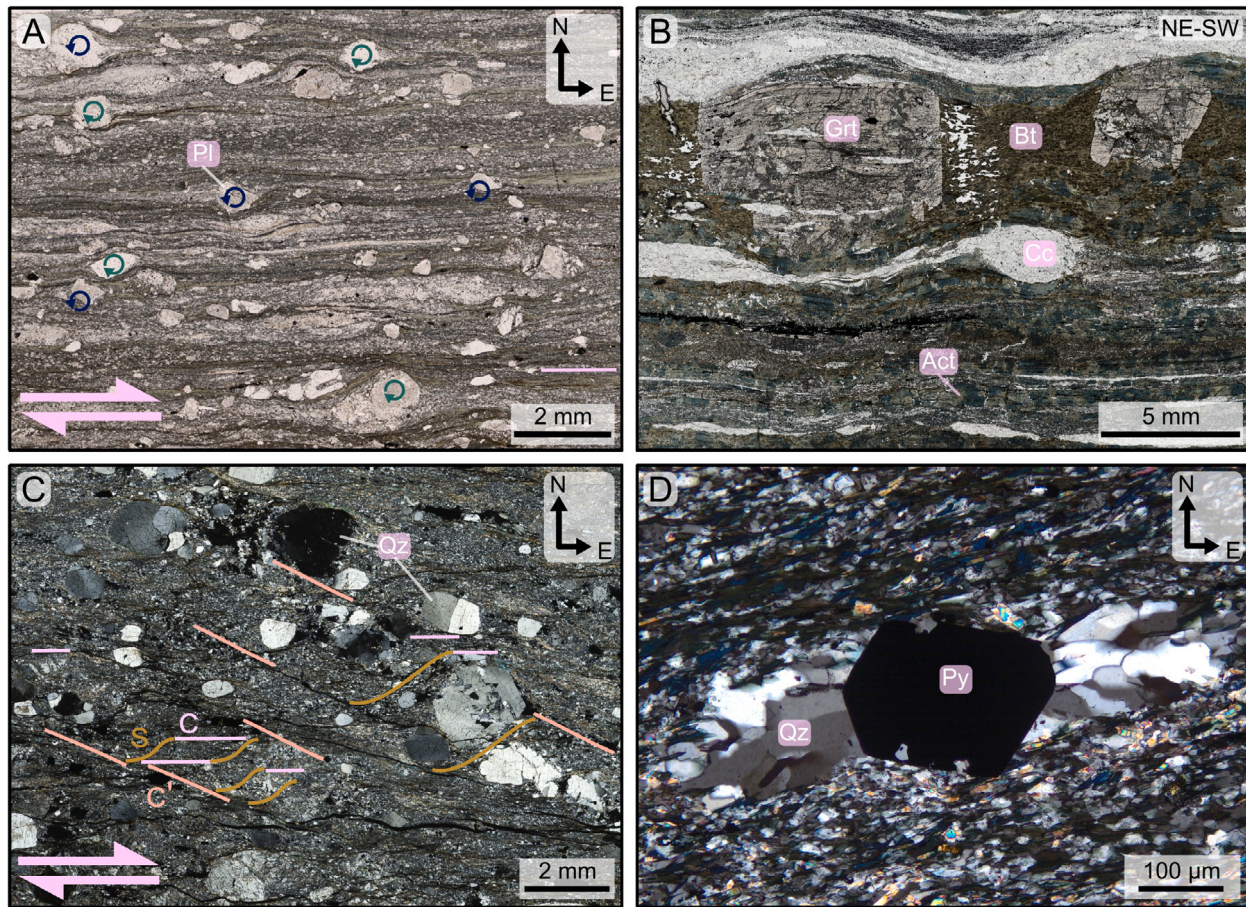


Fig. 5. Microstructures. (A) Mylonite (intermediate meta-volcanic rock) with forward (green arrows) and backward (blue arrows) rotating plagioclase (Pl) porphyroclasts from a dextral shear zone (sample HT-17). Foliation is defined by chlorite. (B) Felsic meta-volcanic rock with tailless garnet (Gt) porphyroclasts. Calcite veins parallel to foliation defined by aligned brown biotite (Bt) and green Fe-rich actinolite (Act) (sample Moss-029). (C) Meta-diorite with dextral SC'-fabric of a chlorite-sericite foliation and tailless quartz (Qz) porphyroclasts (sample Moss-001). (D) Felsic meta-volcanic rock with pyrite (Py) porphyroclast and quartz-tails (sample Moss-045). Thin sections are cut parallel to the macroscopic stretching lineation and perpendicular to the macroscopic foliation.

4.1.4. Gold textures

Gold is observed within foliation-parallel quartz-carbonate-sulfide veins (Figure S1 and S2). The sulfides are mainly pyrite, chalcopyrite, sphalerite, and molybdenite (Figure S2B). Pyrite is porphyroclastic with dissolution-precipitation tails, is inclusion-rich (e.g. calcite, quartz, chalcopyrite, and gold), and fractured. Vein quartz display evidence of intracrystalline deformation (e.g. undulose extinction) and dynamic recrystallization, such as subgrain rotation and bulging recrystallization along quartz-quartz boundaries (Figure S1 and Figure S2A). Gold occurs as inclusions within pyrite (Figure S1, Fig. 2D), as fillings of pyrite microfractures (Figure S2A and D), at the grain-boundary of pyrite (Figure S2B), or disseminated within the deformed vein-quartz.

4.2. Orientation and kinematic analysis

In the Shebandowan Greenstone Belt and the Quetico Subprovince, the foliation is mainly steep and strikes NE-SW, while the stretching lineation is predominantly shallow and parallel to the strike of the foliation (Fig. 7). The metasedimentary units of the Quetico Subprovince are affected by subcylindrical folding (especially at Huronian Lake, HWY-11, and Fortes Lake Road). The associated fold axes are subhorizontal and trend NE-SW, parallel to the stretching lineation in the Shebandowan Greenstone Belt (Fig. 7). This folding is also represented by low uniformity indices for the lineations ($U \approx 0$, i.e. strongly

clustered) and larger U values for the foliation ($U \approx 0.5$, i.e. girdle distribution; Fig. 8).

The variation of the foliation's orientation in the Shebandowan Greenstone Belt is larger relative to the Quetico Subprovince, resulting in higher U values. The dominant NE-SW trend of the lineation remains constant, only the variation in the plunge increases compared to the Quetico Subprovince ($U \approx 0.5$). Towards the SW part of the study area (North and South Burchell Lake Road, Shebandowan Lake, and Whitefish Lake), the stretching lineation rotates towards a more clustered $U \approx 0$ yet subvertical orientation Fig. 8. Associated foliation poles form a shallow, wide girdle distribution suggesting folding around a subvertical axis parallel to the stretching lineation. However, we do not observe evidence for a pre-existing folding event prior to the main deformation event.

The Krige interpolation of foliation strikes (Fig. 9) highlights the predominant NE-SW strike and the relatively small variance in strike (< 0.2). Regions with large variance in strike are concentrated within a narrow zone within the Shebandowan Greenstone Belt close to the south/southeast of the boundary to the Quetico Subprovince. In this region, the foliation deflects from the general NE-SW strike and the trajectories give an anastomosing pattern (i.e. the foliation is deflected by the large felsic plutonic bodies).

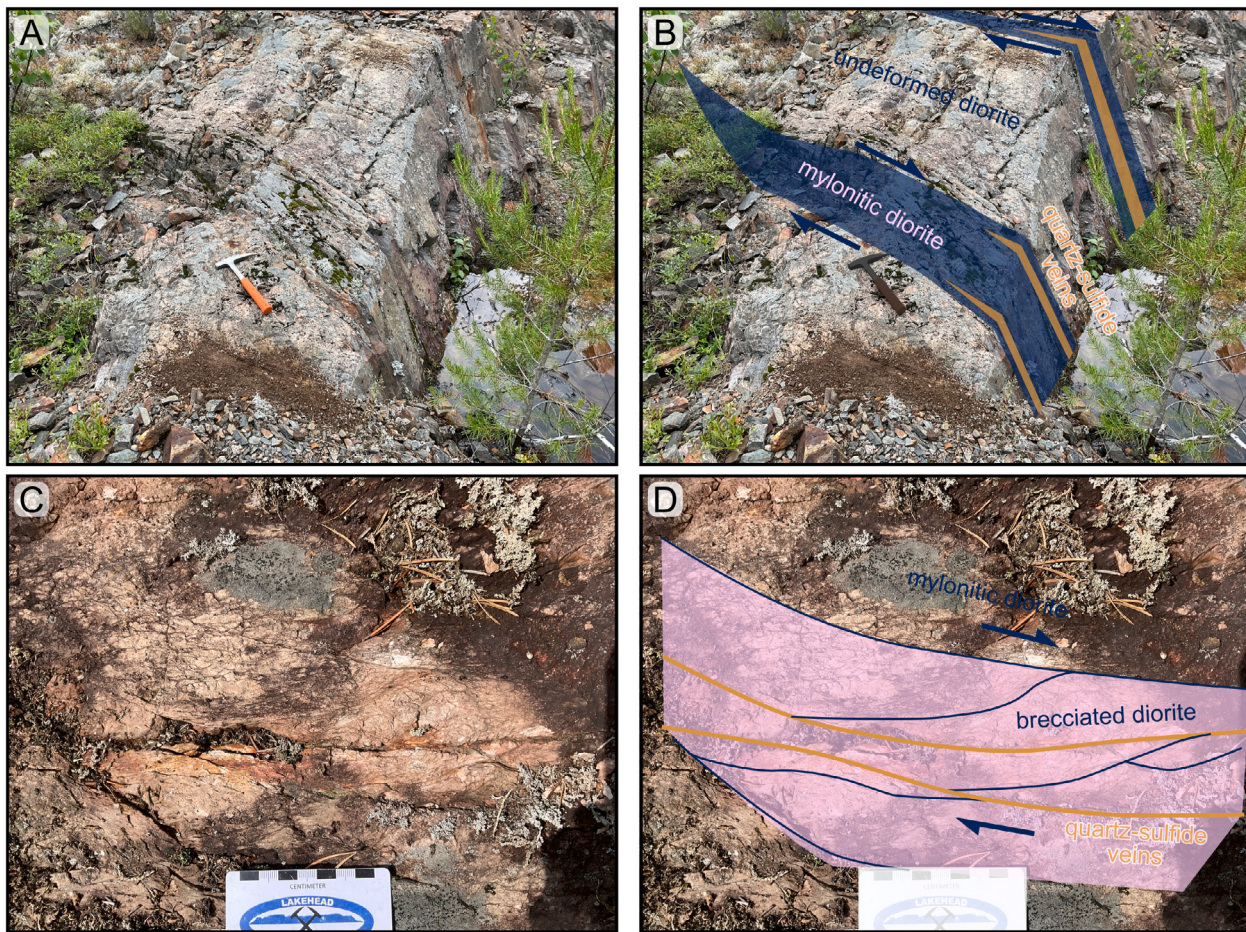


Fig. 6. (A,B) High strain shear zones within diorite (C, D) Close-up of the high strain zone. mylonitic and partly brecciated diorite with quartz-sulfide veins. Location: 90.6684°W, 48.5630°N.

4.3. Vorticity analysis

Estimates of the mean kinematic vorticity number W_m from the rotation of rigid porphyroclasts using the RGN method give values ranging from 0.43 up to 0.85 (Fig. 10). The estimates of W_m suggest that the deformation type ranges from coaxial to non-coaxial dominated flow in the area. The lowest vorticity estimates are measured in samples from the southeastern part of the study area, while the largest estimates are from samples close to the Quetico-Wawa boundary (see Fig. 8).

4.4. Geochronology of felsic intrusive rocks

U-Pb dating of five zircon grains from a syenite sample of the Moss Lake Stock (Fig. 1) yielded a concordia age of 2717.65 ± 0.45 Ma and a weighted mean age of 2717.35 ± 0.48 Ma (Fig. 2). The difference of both age estimates are negligible but the weighted mean age is underdispersed with respect to their analytical measurements (mean square weighted deviation, MSWD < 1).

Re-Os geochronology on molybdenite from an auriferous quartz-vein yielded an age of 2708 ± 12 Ma (supplementary material S2_geochronology.xlsx).

5. Discussion

5.1. Significance of vorticity analyses

Quantifying the shape of the foliation orientation tensor from pooled outcrops (Fig. 8, and Fig. S3) reveals distribution patterns of

foliation and lineation (cluster, girdle, or random) across the study area. The uniformity index of both foliation and lineation varies notably within a narrow zone in the Wawa supprovince close to the subprovince boundary and the gold occurrences. Generally, however, the uniformity profile across the Quetico–Wawa subprovince boundary shows an increase in the uniformity index towards the boundary, from subcylindrical girdle distributions to more strongly clustered foliation poles. This trend reflects the transition from the folded foliation in the SW part of the Quetico Subprovince in the study area towards the dominantly steep foliation at the subprovince boundary. Lineations show a similar trend, from strongly clustered to girdle distributions (Fig. 7), suggesting either superimposed folding or an increase in coaxial deformation during shearing. As we do not observe evidence for re-folding in the field, we interpret that this girdle distribution results from a combination of two lineation clusters produced by vertical simple-shear dominated transpression (resulting in horizontal stretching) and pure-shear dominated transpression (resulting in vertical stretching, Tikoff and Teyssier (1994)). Such a bimodal distribution of vertical and linear lineations yields a U -value of c. 0.5, which can misleadingly resemble a true girdle distribution. Furthermore, our observation of mixed kinematic indicators (i.e. dextral and sinistral shear sense indicators) in the Shebandowan Greenstone Belt also suggests varying contributions of coaxial (pure shear) and non-coaxial (simple shear) deformation.

This interpretation is supported by our vorticity analyses to quantify the kinematic vorticity number. Our estimates for the mean kinematic vorticity number W_m range between 0.1 and 0.9 across the study area (Figs. 10 and 11). In samples where both the RGN and the CVA methods

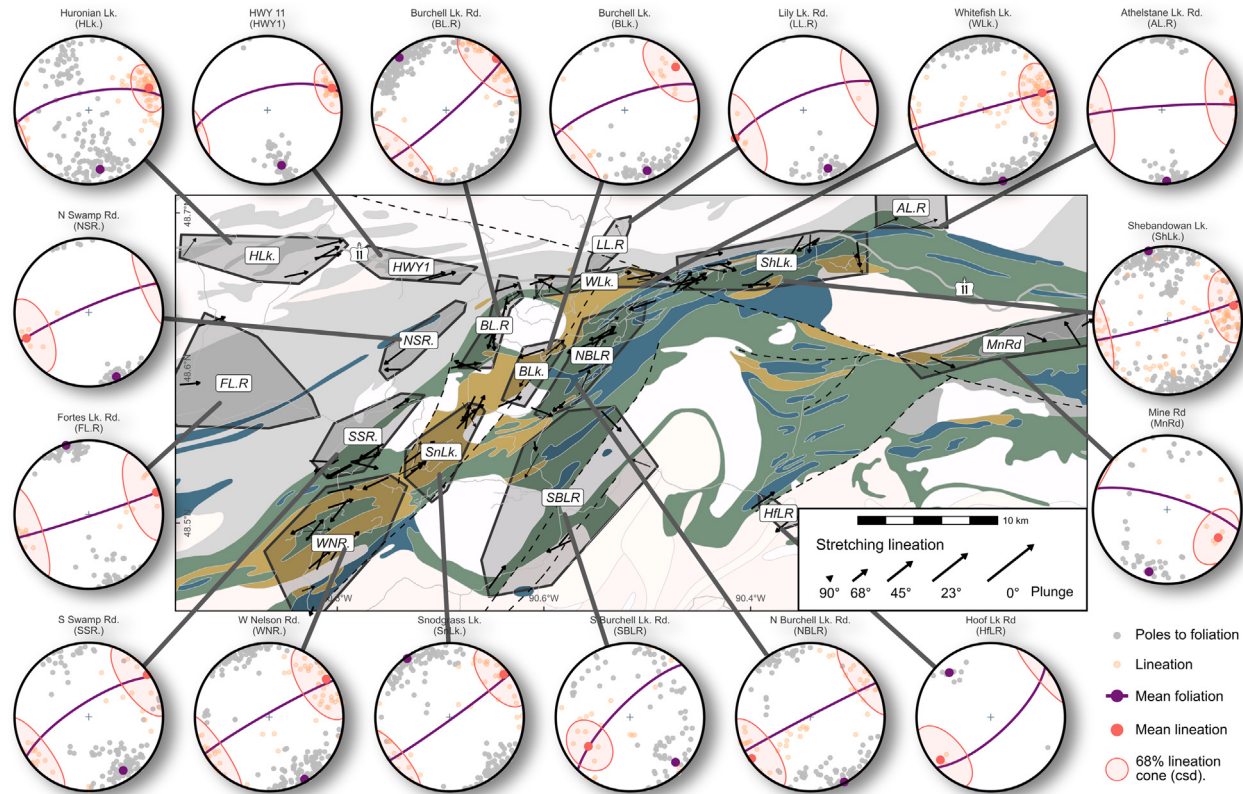


Fig. 7. Simplified map and stereographic projections (equal area, lower hemisphere) for the pooled outcrops. Mean foliation and mean lineation are given by the eigenvectors corresponding to the largest eigenvalues of the orientation matrices of the foliation and lineation (Scheidegger, 1964; Woodcock, 1977; Lisle, 1989). The circular standard deviation of the sphere (csd) is a cone comprising 68% of the data (Mardia and Jupp, 2000). See Fig. 1 for geologic legend.

were applied, the discrepancy between the different estimates is up to 0.4. This discrepancy has been addressed in previous studies (e.g. Law et al., 2004; Xypolias, 2010; Iacopini et al., 2011) and in our case, may be due to a combination of factors, including a low availability of grains in the RGN method, smaller sampling areas in the CVA analyses, the triclinic deformation component in the RGN method, or non-steady state flow during deformation (each described in more detail below).

- Low availability of grains: Stahr and Law (2011) showed that the low availability of grains with a high aspect ratio in a low strain domain can contribute to the underestimation of the W_m values using the RGN method. The low strain effect might have affected our samples because grains with a high aspect ratio (> 4) were rarely measured (Fig. S6). In addition, the RGN method appears to be the most reliable in rocks subjected to moderate finite strains (Grasemann et al., 1999).
- Smaller sampling area for CVA: The CVA vorticity estimates are derived from a smaller sampling area when compared to the RGN method. The latter includes clasts from one or two thin-section (ca. $> 12.4 \text{ cm}^2$), whereas crystallographic vorticity axes are estimated from $< 12.4 \text{ cm}^2$. Effects of small-scale strain partitioning, such as between microlithons and intervening shear bands, may significantly bias estimates of bulk kinematic vorticity from crystallographic orientation data.
- Three-dimensional flow in deformation: A triclinic component of shear causes the mean kinematic vorticity number in the RGN method to underestimate the bulk rocks vorticity number, because the XY plane of the finite strain ellipsoid does not coincide with the VPP (Xypolias, 2010; Iacopini et al., 2008; Kruckenberg

et al., 2019; Iacopini et al., 2011). However, the triclinic component is generally small in our studied rocks, as indicated by the crystallographic vorticity axes (Fig. 11). This suggests that deformation is purely monoclinic within the uncertainties of the measurements, which probably stem mainly from cutting the samples slightly oblique to the lineation-foliation reference frame.

- Non-steady state flow during deformation: The RGN method records the vorticity from feldspar clasts interacting with the rock's matrix, and hence, record a large strain history (see discussion in Xypolias, 2010). In contrast, the CVA method dominantly measures the vorticity from quartz grains, which may only record the final increments of strain. Differences between the vorticity estimates from both methods may thus stem from non-steady state conditions during the flow. In this case, the simple shear component would have increased as deformation progresses, because the W_m estimates from the CVA method are higher than those from the RGN method.

Other fundamental assumptions such as the requirement of clasts embedded in a linear-viscous Newtonian matrix during deformation (i.e. the viscosity is constant, e.g. Johnson et al., 2009a,b), the rigidity of the rotating clasts (recrystallization or fracturing do not change the clasts' shape), the absence of strain-partitioning at the interface between the clast and the matrix, and the initial random orientation of the clasts, may not always be satisfied and thus may also contribute to the discrepancies between the used methods.

Despite these method discrepancies, the scatter of W_m values obtained from outcrops in the Shebandowan Greenstone Belt directly reflects the relative contributions of pure and simple shear during deformation. The spatial distribution of W_m values across the shear

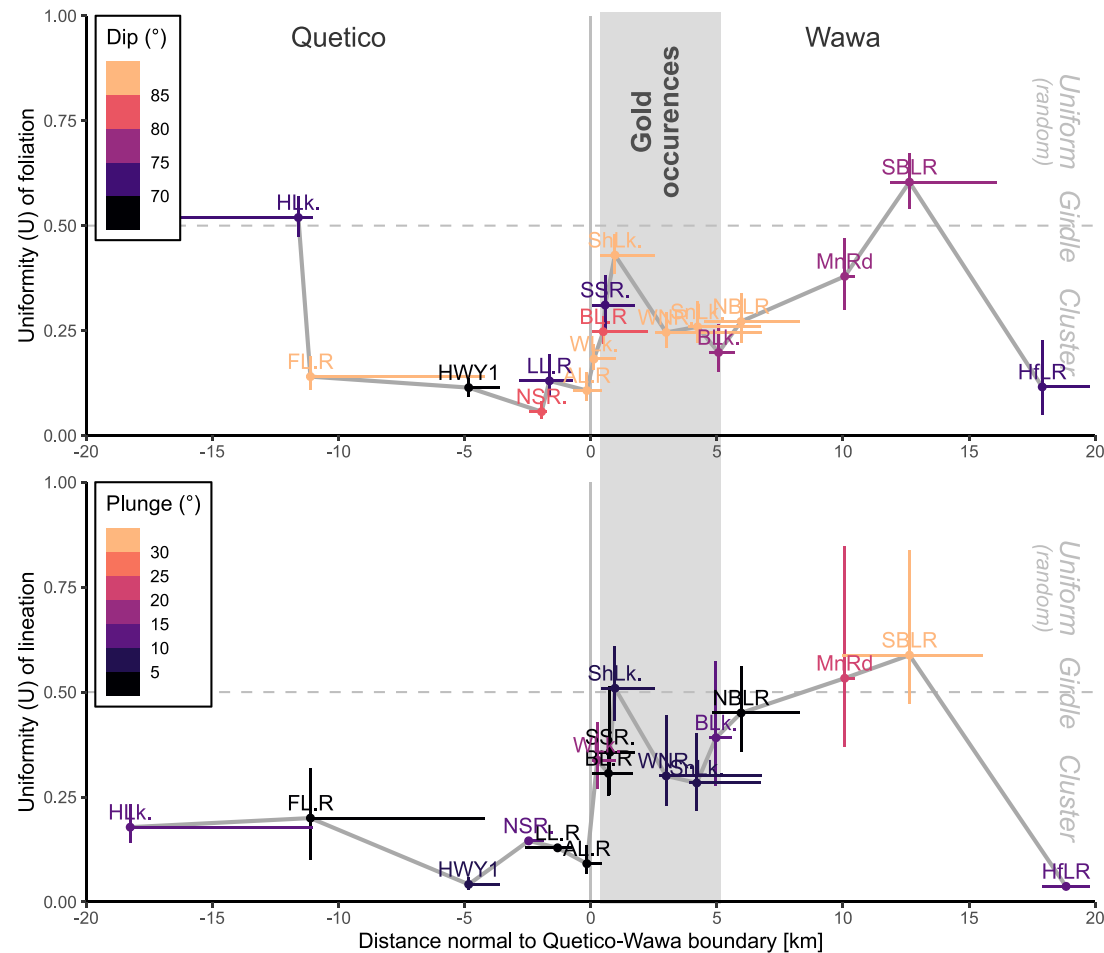


Fig. 8. Uniformity of fabric elements along a profile across the Quetico-Wawa subprovince boundary. The uniformity index is an eigenvalue-based measure for the distribution of orientation data in the pooled outcrops (see Fig. 7). Distances are normal to Quetico-Wawa boundary. Error bars for distance shows the range of distance in each outcrop group while error bars for uniformity index represent the 95% confidence interval of uniformity index estimated from 1000 bootstrap samples.

zone is shown on the vorticity map (Fig. 12A). Although the analyzed 23 samples may not be statistical representative for the study area covering ca. 500 km², the vorticity profile perpendicular to the shear zone reveals notable trends of the mean kinematic vorticity number (Fig. 12B). The highest W_m estimates (> 0.9) are located within a narrow zone (< 4 km wide) in the Shebandowan Greenstone Belt to the southeast of the Quetico and Wawa subprovince boundary. W_m decreases away from this zone reaching the lowest recorded value ($W_m = 0.1$) ca. 12 km to the southeast of the boundary. Furthermore, the mean kinematic vorticity number varies considerably within narrow zones of high strain close to the subprovince boundary.

In conclusion, vorticity estimates demonstrate that the Shebandowan Greenstone Belt is dominated by simple shear near the boundary with the Quetico Subprovince and transitions into a transpressional zone of deformation away from the boundary. This zone of simple shear dominated deformation hosts the main gold deposits which coincide with areas of sudden abrupt changes in the foliation strike (Fig. 9), uniformity index (Fig. 8), and vorticity number (Fig. 12B). The location of these gold occurrences suggests a possible genetic link to foliation bending and vorticity changes but warrants further investigation as most of these occurrences have not been studied in detail.

5.2. Constraints for timing of gold mineralization

Absolute dating of the gold mineralization remains challenging due to the scarcity of dateable minerals definitively associated with gold mineralization and the uncertainties in the Re-Os molybdenite dating. Our Re-Os age yields an age of 2708 ± 12 Ma for molybdenite from a foliation-parallel auriferous quartz vein hosted in metadiorite. However, the veins are deformed and gold shows evidence for remobilization (Fig. S1 and S2). Thus, age estimates for gold's initial mineralization and subsequent remobilization must rely on its relative timing to the large felsic intrusions, the regional metamorphism, and ductile deformation.

Absolute ages based on radiometric dating of zircons and rutile, suggests that the metavolcanic rocks formed at ca. 2720 Ma (Corfu and Stott, 1998) and that the felsic intrusions crystallized around 2690 Ma (Fig. 13; Corfu and Stott, 1998). The undeformed and unmetamorphosed appearance of some felsic intrusions has led to the interpretation that the main deformation event occurred between 2720 Ma and 2690 Ma (Fig. 13). However, this interpretation is at odds with our structural observations and radiometric dating.

We find no evidence of contact metamorphism in the rocks surrounding these intrusions. Instead, we observe dynamic recrystallization in quartz and systematic deflections of the foliation around intrusions, indicative of deformation postdating their emplacement. This

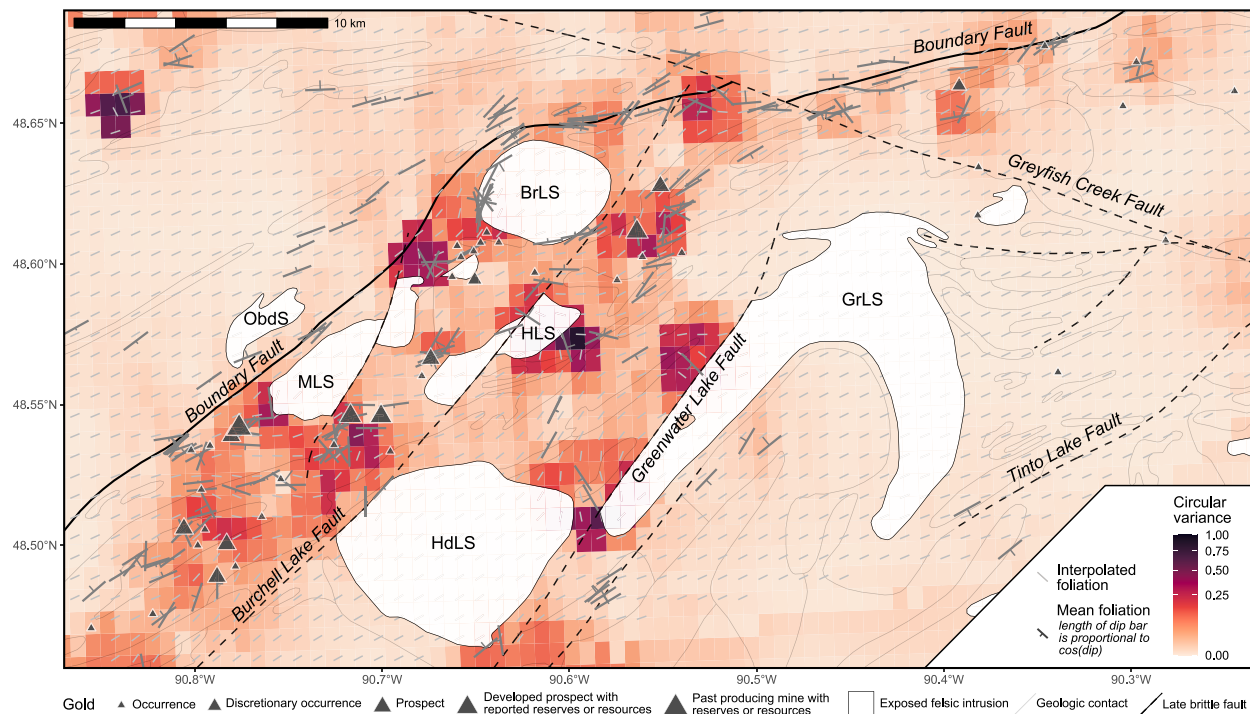


Fig. 9. Variance of interpolated strike of main foliation at surface and distribution of reported gold occurrences (dark gray triangles). Note the spatial concentration of high-grade gold occurrences (larger triangles) surrounding the felsic intrusions (white) as indicated by deflected foliation (high variance > 0.25). The strike is interpolated using circular Kriging of the mean orientation ($n=227$) of the foliation observed at each outcrop. See Fig. 1 for abbreviated names of felsic intrusions.

is in agreement with our zircon U-Pb TIMS age of a macroscopically undeformed syenite from the Moss Lake Stock (2717 ± 0.5 Ma; Figs. 1 and 2), pre-dating the previously suggested timing of regional metamorphism and ductile deformation.

Moreover, rocks of the Quetico Subprovince underwent comparable deformation and metamorphic conditions to those in the Shebandowan Greenstone Belt. The maximum deposition age (youngest zircon) for the metasedimentary rocks in the Quetico Subprovince is 2700–2690 Ma, followed by peak metamorphism at ca. 2671–2665 Ma (Fig. 13; Pan et al., 1998; Corfu, 2000). This suggests that the Shebandowan Greenstone Belt was still affected by metamorphism and ductile deformation approximately 20 Myr after the felsic intrusive magmatism. This timing is consistent with constraints on exhumation from amphibolite-facies conditions occurring between 2678 and 2668 Ma (Ar-Ar geochronology) at the easternmost extension of the subprovince boundary in Québec (here Abitibi-Opatica boundary; Daoudene et al., 2022).

Comparing our Re-Os molybdenite age with the compiled ages constraining the timing of magmatism reveals that gold-associated molybdenite mineralization overlaps with two phases of felsic magmatism (Shebandowan and Greenwater phases of magmatism; Fig. 13). Although the uncertainties in the Re-Os age do not allow precise relationship to one of these magmatic phases, the age coincides with the exhumation age. Moreover, as the gold- and molybdenite bearing veins are parallel to the main foliation and show evidence for deformation (Fig. S1 and S2), the Re-Os molybdenite age likely predates the latest stage of gold enrichment, which we interpret to have occurred syn-deformation in a window between 2690 (i.e., timing of the deposition of the Quetico metasedimentary protoliths) and 2665 Ma (i.e., timing of regional exhumation).

5.3. Structural and microstructural evidence for syn-deformational gold deposition

Active faults and shear zones play a critical role in vein emplacement by enhancing fracture formation. Deformation within active shear and fault zones significantly increases local permeability, favoring the redistribution of large volumes of hydrothermal fluids and focusing fluid flow (Cox et al., 2001; Campbell McCuaig and Kerrich, 1998; Faulkner et al., 2010). This channeling of fluid flow in high-strain zones has been critical in the formation of numerous world-class and giant lode gold deposits along such structures (Goldfarb et al., 2005; Groves et al., 1995, 2018; Blenkinsop and Doyle, 2014).

In the Shebandowan Greenstone Belt, gold-bearing quartz-carbonate-sulfide veins are mainly oriented parallel to the main foliation of mylonite rocks where the steep ore shoots are perpendicular to the dominant shallowly plunging lineation within the foliation plane (Osmani, 1997). It, therefore, seems that the emplacement and the growth of aqueous-carbonaceous auriferous quartz-sulfide veins occurred during periods of active deformation under relatively low-temperature conditions (greenschist-facies metamorphism). Our field relations and microstructural analysis agree that mylonitic fabrics in gold-bearing quartz veins and host rocks were formed coevally during low-temperature ductile deformation, as evidenced by dynamic recrystallization of quartz, brittle deformation of feldspar, and rotated rigid sulphides with asymmetric quartz pressure-solution tails (Figs. 6 and S2).

5.4. Controls on gold distribution: foliation deflection, vorticity and strain partitioning

Foliation strike and vorticity analyses reveal that gold in the western Shebandowan Greenstone Belt (Wawa-Abitibi Province) is preferentially concentrated along deflected high-strain shear zones with

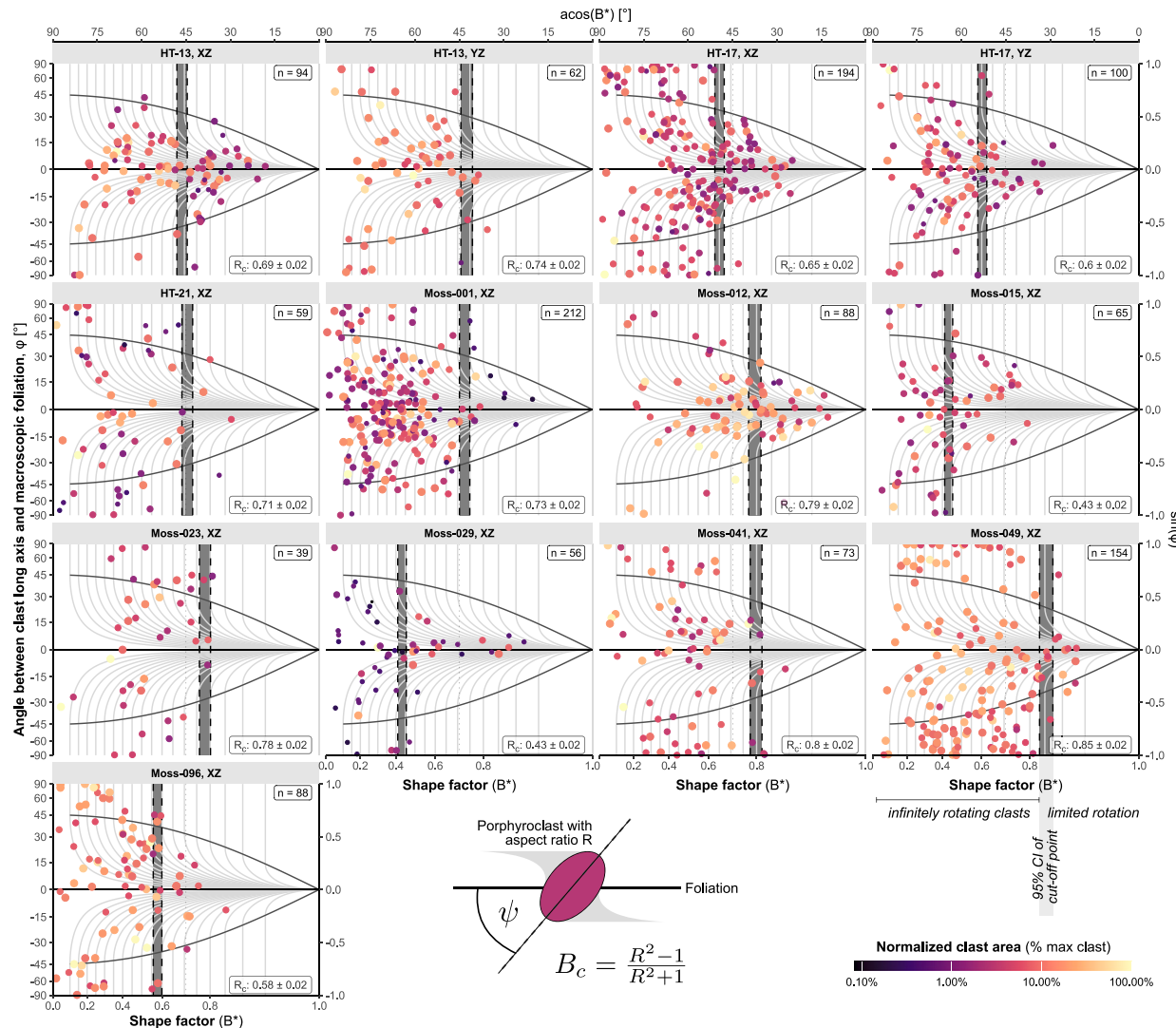


Fig. 10. Vorticity analyses of 13 specimens based on the rigid grain net method of Jessup et al. (2007). The shape factor B_c is a function of the aspect ratio of the porphyroblast (Eq. (3)). Vertical, dashed gray lines show the 95% confidence interval for the boundary between infinitely rotating porphyroblasts and those that have entered a “stable sink” position (limited rotation). n — number of clasts.

substantial non-coaxial (simple-shear) deformation (e.g. Leclair et al., 1993). In particular, gold accumulates in zones of vorticity change, where strain is partitioned between simple-shear- and pure-shear dominated deformation (Figs. 9 and 12). Similar spatial associations between vorticity changes and gold concentration have been reported in shear zone hosted quartz vein lode-gold deposits in the Borborema Province in Brazil (de Almeida et al., 2024), the Eastern Dharwar Craton of southern India (Kar et al., 2024), and the Eastern desert of Egypt (Kassem et al., 2016).

In the Shebandowan Greenstone Belt, foliation deflections and strain partitioning occur near large felsic intrusions predating the mylonitic fabric and metamorphism (Fig. 13). These syenitic, monzonitic and dioritic intrusions are feldspar-rich with isotropic fabrics (Fig. S7), and are therefore rheologically stronger than the surrounding quartz-rich and anisotropic metavolcanic rocks. Acting as rigid bodies during ductile deformation, they cause foliation deflections and strain partitioning at various scales. Gold enrichment appears to be primarily localized near large-scale intrusive bodies, as shown by the spatial distribution of major gold occurrences (Fig. 1).

Field evidence of dilatational jogs and restraining bends near low-strain rigid bodies supports the interpretation that competency contrasts drive fabric deflections and strain partitioning (Fig. 6). Dilatational jogs create fluid pathways by reducing effective mean stresses

(overpressure), promoting brittle deformation (e.g. Cox, 2005; Connolly and Cosgrove, 1999a,b). Restraining bends (contractional fault jogs) lead to extensive brecciation and may also promote permeability (Rispoli, 1981; Sibson, 1986; Kim et al., 2004). Both structures can create a positive feedback loop, where high permeability facilitates continuous fluid migration, reducing mean stresses and causing further fracture damage in the jogs (Sibson et al., 1988). This process can lead to the development of multi-event overprinting vein systems, with individual veins oriented normal to local extension directions (Lee and Wiltschko, 2000). Thereby, multiple generations of fluids may blur any geochemical signal tying the gold to its source-fluid composition.

Dilatational and contractional jogs in a vertical shear zone enable vertical fluid migration of gold-bearing aqueous-carbonaceous fluids derived from deeper Archean basement rocks undergoing partial melting or prograde metamorphism (e.g. Goldfarb and Pitcairn, 2023). Secondary gold enrichment may then occur through remobilization due to dissolution-precipitation (Hastie et al., 2020; Fougerousse et al., 2016) or dynamic recrystallization of quartz and sulfides (e.g. Dubosq et al., 2018), followed by re-precipitation in response to temperature or fluid chemistry changes in low mean stress areas (e.g. Cox et al., 1995). Fluid overpressure-induced seismic activity in these jogs and the piezoelectric effects in quartz may further enhance gold concentration (Voisey et al., 2024).

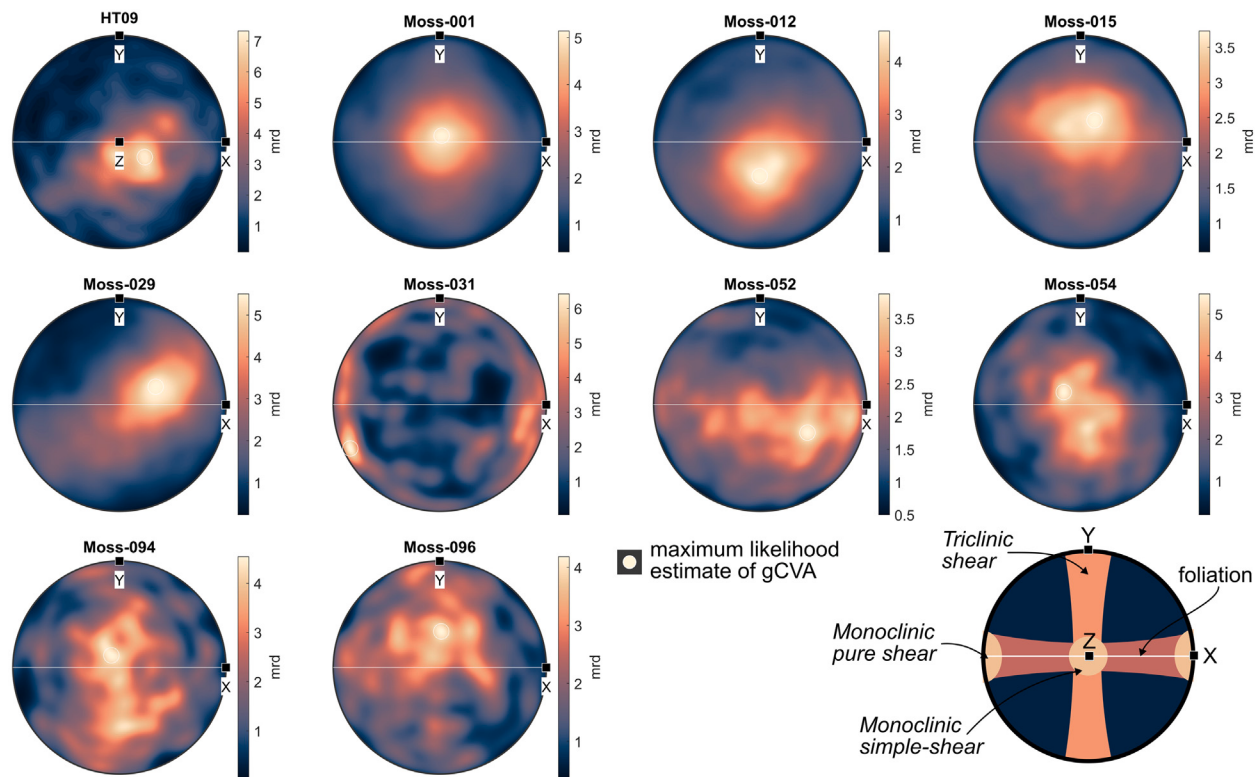


Fig. 11. Crystallographic vorticity axes in sample coordinate system XYZ (X — stretching lineation, Y — normal to foliation, Z — direction of observer; equal-area stereographic projection into upper hemisphere). mrd — multiples of random distribution (kernel halfwidth: 7.5°).

Since many gold deposits in the Superior Craton are associated with regional Archean dextral transpression (e.g. Leclair et al., 1993; Card et al., 1989; Poulsen et al., 1992; Jellicoe et al., 2022; Lin, 2001; Muir, 2003; Lafrance et al., 2004; Tóth et al., 2023; Lin and Corfu, 2002; Müller et al., 2021; Zammit et al., 2022; Sibson et al., 1988), we propose that gold mineralization along the peripheries of rigid felsic intrusions in domains of simple shear dominated deformation may be an intrinsic feature of granite greenstone belts. Mapping vorticity changes and quantifying foliation deflections could thus serve as a powerful and cost-effective tool for gold exploration.

6. Conclusions

Gold mineralization in the western Shebandowan Greenstone Belt is associated with ductile shear zones near the boundary with the Quetico Subprovince. These gold occurrences are closely linked to changes in the orientation of the ductile foliation within metavolcanic units adjacent to felsic intrusive bodies. The competency contrast between the metavolcanic units and feldspar-rich, isotropic intrusive bodies causes the foliation to deflect, leading to localized strain partitioning between coaxial (pure shear) and non-coaxial (simple shear) domains. This partitioning is reflected in variations of the kinematic vorticity numbers — a measure for the degree of coaxiality in the ductile flow. Localized strain partitioning along the deflected foliation forms releasing (dilatational jogs) and restraining bands (contractional jogs). These structures create vertical fluid pathways and stress accumulation, culminating in brittle deformation and permeability. These processes promote multiple episodes of fluid migration as well as local remobilization of gold, required to upscale the gold concentration to economic levels.

CRediT authorship contribution statement

Tobias Stephan: Writing – review & editing, Writing – original draft, Visualization, Validation, Software, Methodology, Investigation, Formal analysis, Data curation, Conceptualization. **Noah J.**

Phillips: Writing – review & editing, Writing – original draft, Validation, Methodology, Funding acquisition, Conceptualization. **Hanna Tiitto:** Writing – original draft, Investigation, Data curation. **Adrian Perez:** Investigation. **Michael Nwakanma:** Investigation. **Robert Creaser:** Validation, Methodology, Investigation, Data curation. **Pete Hollings:** Writing – review & editing, Writing – original draft, Project administration, Funding acquisition, Formal analysis, Conceptualization.

Declaration of competing interest

The authors declare the following financial interests/personal relationships which may be considered as potential competing interests: Tobias Stephan, Noah Phillips, Peter Hollings report financial support was provided by Natural Sciences and Engineering Research Council of Canada. If there are other authors, they declare that they have no known competing financial interests or personal relationships that could have appeared to influence the work reported in this paper.

Acknowledgments

This research was funded through NSERC Alliance Grant [ALLRP 571052 - 21]. We are grateful for support from a Mitacs Accelerate grant. H. T. received funding from the SEG research award. N. P. was funded through a NSERC Discovery grant. Paris Xypolias and an anonymous reviewer are thanked for the valuable comments and suggestions to improve the manuscript. We thank Jason Pattison, Mark Wellstead, and Peter Flindell from Goldshore Resources Inc. for granting access to the study area and providing logistical support. We also thank Sudip Shrestha (Fipke Laboratory for Trace Element Research The University of British Columbia - Okanagan) for technical assistance. Finally, we are grateful to Zach Michels and Mary Louise Hill for their stimulating discussions, which significantly enriched the interpretation of this study.

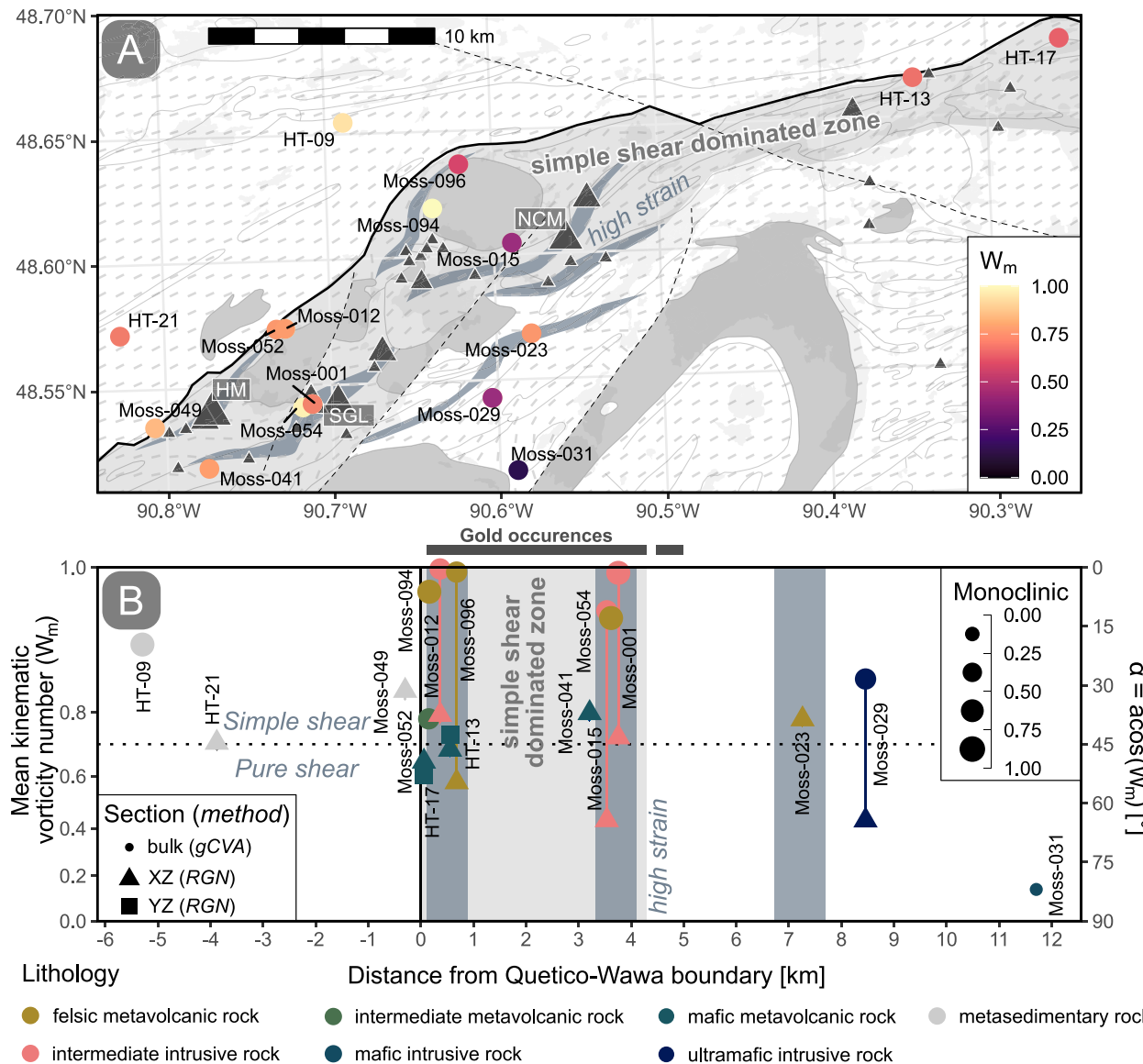


Fig. 12. Vorticity across the Quetico-Wawa subprovince boundary. (A) Spatial distribution of the mean kinematic vorticity numbers W_m . Gray triangles show known gold occurrences, gray areas show surface exposure of felsic granitoids, and gray bars show the strike of the main foliation (see Fig. 9 for details). Gold deposits: HM — Huronian Mine (inactive), NCM — North Coldstream Mine (inactive), SGL — Snodgrass Lake deposit. (B) NW-SE profile showing the mean kinematic vorticity numbers and their distances normal to Quetico-Wawa subprovince boundary. Note the increase of simple shear within high-strain zones, and the lower W_m outside of these zones and within strain shadows of larger intrusive bodies. The monoclinic score indicates the amount of monoclinic flow geometry and ranges from 0 for triclinic shear to 1 for monoclinic shear. The angle α between the flow apophyses is $>45^\circ$ for pure shear dominated general shear and $<45^\circ$ for simple shear dominated general shear.

Appendix A. Supplementary data

Supplementary material related to this article can be found online at <https://doi.org/10.1016/j.jsg.2025.105542>.

Data availability

The structural data and field notes are available through the StraboSpot project repository in [10.17605/OSF.IO/C4EY9](https://doi.org/10.17605/OSF.IO/C4EY9).

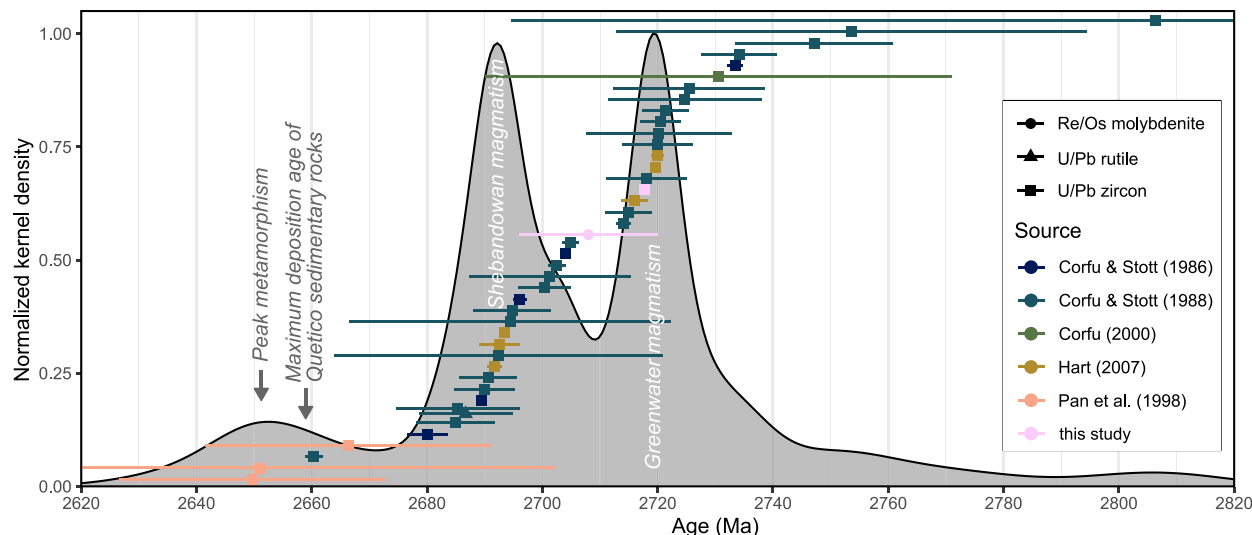


Fig. 13. Geochronological compilation of Shebandowan Greenstone Belt showing the mean ages and their 2σ standard deviation. Grey spectrum shows the adaptive, weighted kernel density estimate of the compiled ages (details in Tab. S2).

References

- Arslan, A., Passchier, C.W., Koehn, D., 2008. Foliation boudinage. *J. Struct. Geol.* 30 (3), 291–309. <http://dx.doi.org/10.1016/j.jsg.2007.11.004>.
- Ayer, J., Amelin, Y., Corfu, F., Kamo, S., Ketchum, J., Kwok, K., 2002. Evolution of the southern Abitibi greenstone belt based on U-Pb geochronology: autochthonous volcanic construction followed by plutonism, regional deformation and sedimentation. *Precambrian Res.* 115, 63–95.
- Ayer, J.A., Thurston, P.C., Bateman, R., Dubé, B., Gibson, H.L., Hamilton, M.A., Hathway, B., Hocker, S.M., Houlé, M.G., Hudak, G., Ispolatov, V.O., Lafrance, B., Lesher, C.M., MacDonald, P.J., Pélouquin, A.S., Piercy, S.J., Reed, L.E., Thomson, P.H., 2005. Overview of results from the greenstone architecture project. *Discover Abitibi Initiative. Open File Report*, 6154.
- Bachmann, F., Hielscher, R., Schaeben, H., 2010. Texture analysis with MTEX – Free and open source software toolbox. *Solid State Phenom.* 160, 63–68. <http://dx.doi.org/10.4028/www.scientific.net/SSP.160.63>.
- Blenkinsop, T.G., Doyle, M.G., 2014. Structural controls on gold mineralization on the margin of the yilgarn craton, Albany-Fraser orogen: The Tropicana deposit, Western Australia. *J. Struct. Geol.* 67, 189–204. <http://dx.doi.org/10.1016/j.jsg.2014.01.013>.
- Blenkinsop, T.G., Oliver, N.H.S., Dirks, P.G.H.M., Nugus, M., Tripp, G., Sanislav, I., 2020. Chapter 1: Structural geology applied to the evaluation of hydrothermal gold deposits. In: Applied Structural Geology of Ore-Forming Hydrothermal Systems. Society of Economic Geologists, pp. 1–23. <http://dx.doi.org/10.5382/rev.21.01>.
- Borradaile, G.J., 1978. Transected folds: A study illustrated with examples from Canada and Scotland. *Geol. Soc. Am. Bull.* 89 (4), 481. [http://dx.doi.org/10.1130/0016-7606\(1978\)89<481:tfasiw>2.0.co;2](http://dx.doi.org/10.1130/0016-7606(1978)89<481:tfasiw>2.0.co;2).
- Borradaile, G.J., Schwerdtner, W.M., 1984. Horizontal shortening of upward-facing greenstone structures in the southern Superior Province, Canadian shield. *Can. J. Earth Sci.* 21 (5), 611–615. <http://dx.doi.org/10.1139/e84-066>.
- Borradaile, G., Spark, R., 1991. Deformation of the Archean Quetico-Shebandowan subprovince boundary in the Canadian Shield near Kashabowie, northern Ontario. *Can. J. Earth Sci.* 28 (1), 116–125. <http://dx.doi.org/10.1139/e91-010>.
- Burrows, D.R., Spooner, E.T.C., 1987. Generation of a magmatic H_2O-CO_2 fluid enriched in Au, Mo, and W within an Archean sodic granodiorite stock, Mink Lake, northwestern Ontario. *Econ. Geol.* 82 (7), 1931–1957. <http://dx.doi.org/10.2113/gsecongeo.82.7.1931>.
- Campbell McCuaig, T., Kerrich, R., 1998. P-T-t-deformation-fluid characteristics of lode gold deposits: evidence from alteration systematics. *Ore Geol. Rev.* 12 (6), 381–453. [http://dx.doi.org/10.1016/S0169-1368\(98\)80002-4](http://dx.doi.org/10.1016/S0169-1368(98)80002-4).
- Card, K.D., Poulsen, K.H., Robert, F., 1989. The archean superior province of the Canadian shield and its lode gold deposits. In: Keays, R.R., Ramsay, W.R.H., Groves, D.I. (Eds.), *The Geology of Gold Deposits: The Perspective in 1988*. Society of Economic Geologists, pp. 19–36. <http://dx.doi.org/10.5382/mono.06.02>.
- Carter, M.W., 1984. Goldie and horne townships, district of thunder bay. In: *Summary of Field Work 1984, Ontario Miscellaneous Survey*. In: *Ontario Geological Survey Miscellaneous Paper*, vol. 119, Ontario Geological Survey, pp. 41–45.
- Connolly, P., Cosgrove, J., 1999a. Prediction of fracture-induced permeability and fluid flow in the crust using experimental stress data. *AAPG Bull.* 83 (1999), 104720. <http://dx.doi.org/10.1306/e4fd2d75-1732-11d7-8645000102c1865d>.
- Connolly, P., Cosgrove, J., 1999b. Prediction of static and dynamic fluid pathways within and around dilational jogs. *Geol. Soc. Lond. Spec. Publ.* 155 (1), 105–121. <http://dx.doi.org/10.1144/gsl.sp.1999.155.01.09>.
- Corfu, F., 2000. Extraction of Pb with artificially too-old ages during stepwise dissolution experiments on Archean zircon. *Lithos* 53 (3–4), 279–291. [http://dx.doi.org/10.1016/S0024-4937\(00\)00030-X](http://dx.doi.org/10.1016/S0024-4937(00)00030-X).
- Corfu, F., Stott, G.M., 1986. U-Pb ages for late magmatism and regional deformation in the Shebandowan Belt, Superior Province, Canada. *Can. J. Earth Sci.* 23 (8), 1075–1082. <http://dx.doi.org/10.1139/e86-108>.
- Corfu, F., Stott, G.M., 1998. Shebandowan greenstone belt, western Superior Province: U-Pb ages, tectonic implications, and correlations. *Bull. Geol. Soc. Am.* 110 (11), 1467–1484. [http://dx.doi.org/10.1130/0016-7606\(1998\)110<1467:SGBWSP-2.3.CO;2](http://dx.doi.org/10.1130/0016-7606(1998)110<1467:SGBWSP-2.3.CO;2).
- Cox, S.F., 2005. Coupling between deformation, fluid pressures, and fluid flow in ore-producing hydrothermal systems at depth in the crust. In: One Hundredth Anniversary Volume. Society of Economic Geologists, <http://dx.doi.org/10.5382/av100.04>.
- Cox, S.F., 2016. Injection-driven swarm seismicity and permeability enhancement: Implications for the dynamics of hydrothermal ore systems in high fluid-flux, overpressured faulting regimes—An invited paper. *Econ. Geol.* 111 (3), 559–587. <http://dx.doi.org/10.2113/econgeo.111.3.559>.
- Cox, F., Knackstedt, M.A., Braun, J., 2001. Principles of structural control on permeability and fluid flow in hydrothermal systems. In: Richards, J.P., Tosdal, R.M. (Eds.), In: *Structural Controls on Ore Genesis*, vol. 14, Society of Economic Geologists, pp. 1–24. <http://dx.doi.org/10.5382/rev.14.01>.
- Cox, S.F., Sun, S.S., Etheridge, M.A., Wall, V.J., Potter, T.F., 1995. Structural and geochemical controls on the development of turbidite-hosted gold quartz vein deposits, Wattle Gully Mine, central Victoria, Australia. *Econ. Geol.* 90 (6), 1722–1746. <http://dx.doi.org/10.2113/gsecongeo.90.6.1722>.
- Cox, S.F., Wall, V.J., Etheridge, M.A., Potter, T.F., 1991. Deformational and metamorphic processes in the formation of mesothermal vein-hosted gold deposits - examples from the Lachlan Fold Belt in central Victoria, Australia. *Ore Geol. Rev.* 6 (5), 391–423. [http://dx.doi.org/10.1016/0169-1368\(91\)90038-9](http://dx.doi.org/10.1016/0169-1368(91)90038-9).
- Daoudene, Y., Tremblay, A., Ruffet, G., Leclerc, F., 2022. The Abitibi-Opatica transition, Superior Province, Quebec, Canada: Structural analysis, 40Ar/39Ar thermochronology and implications for Archean tectonics. *Precambrian Res.* 379, 106803. <http://dx.doi.org/10.1016/j.precamres.2022.106803>.
- Davis, W.J., Lacroix, S., Gariépy, C., Machado, N., 2000. Geochronology and radiogenic isotope geochemistry of plutonic rocks from the central Abitibi subprovince: significance to the internal subdivision and plutono-tectonic evolution of the Abitibi belt. *Can. J. Earth Sci.* 37 (2–3), 117–133. <http://dx.doi.org/10.1139/e99-093>.
- Davis, D.W., Pezzutto, F., Ojakangas, R.W., 1990. The age and provenance of metasedimentary rocks in the Quetico Subprovince, Ontario, from single zircon analyses: implications for Archean sedimentation and tectonics in the Superior Province. *Earth Planet. Sci. Lett.* 99 (3), 195–205. [http://dx.doi.org/10.1016/0012-821X\(90\)90110-J](http://dx.doi.org/10.1016/0012-821X(90)90110-J).
- de Almeida, H.L., Misas, C.M.E., dos Santos Teles, G., 2024. Microfabric, 3D-strain geometry and kinematic vorticity analysis of Au-bearing shear zone, Central Domain of the Borborema Province, NE Brazil. *J. South Am. Earth Sci.* 133 (November 2023), 104720. <http://dx.doi.org/10.1016/j.jsames.2023.104720>.

- Dubosq, R., Lawley, C.J.M., Rogowitz, A., Schneider, D.A., Jackson, S., 2018. Pyrite deformation and connections to gold mobility: Insight from micro-structural analysis and trace element mapping. *Lithos* 310–311, 86–104. <http://dx.doi.org/10.1016/j.lithos.2018.03.024>.
- Dufresne, M., Black, W., 2024. Technical Report and Updated Mineral Resource Estimate for the Moss Gold Project, Ontario, Canada. Technical Report, APEX Geoscience Ltd.
- Duuring, P., Cassidy, K.F., Hagemann, S.G., 2007. Granitoid-associated orogenic, intrusion-related, and porphyry style metal deposits in the Archean Yilgarn Craton, Western Australia. *Ore Geol. Rev.* 32 (1–2), 157–186. <http://dx.doi.org/10.1016/j.oregeorev.2006.11.001>.
- Faulkner, D.R., Jackson, C.A.L., Lunn, R.J., Schlische, R.W., Shipton, Z.K., Wibberley, C.A.J., Withjack, M.O., 2010. A review of recent developments concerning the structure, mechanics and fluid flow properties of fault zones. *J. Struct. Geol.* 32 (11), 1557–1575. <http://dx.doi.org/10.1016/j.jsg.2010.06.009>.
- Fougerousse, D., Micklethwaite, S., Tomkins, A.G., Mei, Y., Kilburn, M., Guagliardo, P., Fisher, L.A., Halfpenny, A., Gee, M., Paterson, D., Howard, D.L., 2016. Gold remobilisation and formation of high grade ore shoots driven by dissolution-reprecipitation replacement and Ni substitution into auriferous arsenopyrite. *Geochim. Cosmochim. Acta* 178, 143–159. <http://dx.doi.org/10.1016/j.gca.2016.01.040>.
- Fralick, P.W., Kronberg, B.I., 1997. Geochemical discrimination of clastic sedimentary rock sources. *Sediment. Geol.* 113 (1–2), 111–124. [http://dx.doi.org/10.1016/S0037-0738\(97\)00049-3](http://dx.doi.org/10.1016/S0037-0738(97)00049-3).
- Fralick, P., Pufahl, P.K., 2006. Iron formation in Neoarchean Deltaic successions and the microbially mediated deposition of transgressive systems tracts. *J. Sediment. Res.* 76 (9), 1057–1066. <http://dx.doi.org/10.2110/jsr.2006.095>.
- Frieman, B.M., Kuiper, Y.D., Kelly, N.M., Monecke, T., Kylander-Clark, A., 2017. Constraints on the geodynamic evolution of the southern Superior Province: U-Pb LA-ICP-MS analysis of detrital zircon in successor basins of the Archean Abitibi and Pontiac subprovinces of Ontario and Quebec, Canada. *Precambrian Res.* 292, 398–416. <http://dx.doi.org/10.1016/j.precamres.2017.01.027>.
- Frimmel, H.E., 2008. Earth's continental crustal gold endowment. *Earth Planet. Sci. Lett.* 267 (1–2), 45–55. <http://dx.doi.org/10.1016/j.epsl.2007.11.022>.
- Frost, B.R., Mavrogenes, J.A., Tomkins, A.G., 2002. Partial melting of sulfide ore deposits during medium and high-grade metamorphism. *Can. Miner.* 40 (February), 1–18. <http://dx.doi.org/10.2113/gscannin.40.1.1>.
- Ghosh, S.K., Ramberg, H., 1976. Reorientation of inclusions by combination of pure shear and simple shear. *Tectonophysics* 34 (1–2), 1–70. [http://dx.doi.org/10.1016/0040-1951\(76\)90176-1](http://dx.doi.org/10.1016/0040-1951(76)90176-1).
- Giblin, P.E., 1964. *Geology of the Burchell Lake area, District of Thunder Bay*. Tech. Rep. 19, Ontario Department of Mines.
- Gold, T., Soter, S., 1984. Fluid ascent through the solid lithosphere and its relation to earthquakes. *Pure Appl. Geophys.* 122 (2–4), 492–530. <http://dx.doi.org/10.1007/bf00874614>.
- Goldfarb, R.J., Baker, T., Dubé, B., Groves, D.I., Hart, C.J.R., Gosselin, P., 2005. Distribution, character, and genesis of gold deposits in metamorphic terrane. In: One Hundredth Anniversary Volume. Society of Economic Geologists, pp. 407–450. <http://dx.doi.org/10.5382/AV100.14>.
- Goldfarb, R.J., Groves, D.I., 2015. Orogenic gold: Common or evolving fluid and metal sources through time. *Lithos* 233, 2–26. <http://dx.doi.org/10.1016/j.lithos.2015.07.011>.
- Goldfarb, R.J., Pitcairn, I., 2023. Orogenic gold: is a genetic association with magmatism realistic? *Miner. Deposita* 58 (1), 5–35. <http://dx.doi.org/10.1007/s00126-022-01146-8>.
- Grasemann, B., Fritz, H., Vannay, J.-C., 1999. Quantitative kinematic flow analysis from the Main Central Thrust Zone (NW-Himalaya, India): implications for a decelerating strain path and the extrusion of orogenic wedges. *J. Struct. Geol.* 21 (7), 837–853. [http://dx.doi.org/10.1016/s0191-8141\(99\)00077-2](http://dx.doi.org/10.1016/s0191-8141(99)00077-2).
- Groves, D.I., Goldfarb, R.J., Gebre-Mariam, M., Hagemann, S.G., Robert, F., 1998. Orogenic gold deposits: A proposed classification in the context of their crustal distribution and relationship to other gold deposit types. *Ore Geol. Rev.* 13 (1–5), 7–27. [http://dx.doi.org/10.1016/s0169-1368\(97\)00012-7](http://dx.doi.org/10.1016/s0169-1368(97)00012-7).
- Groves, D.I., Ridley, J.R., Bloem, E.M.J., Gebre-Mariam, M., Hagemann, S.G., Hronsky, J.M.A., Knight, J.T., McNaughton, N.J., Ojala, J., Vielreicher, R.M., McCuaig, T.C., Holyland, P.W., 1995. Lode-gold deposits of the Yilgarn block: products of Late Archean crustal-scale overpressured hydrothermal systems. *Geol. Soc. Lond. Spec. Publ.* 95 (1), 155–172. <http://dx.doi.org/10.1144/gsl.sp.1995.095.01.10>.
- Groves, D.I., Santosh, M., Goldfarb, R.J., Zhang, L., 2018. Structural geometry of orogenic gold deposits: Implications for exploration of world-class and giant deposits. *Geosci. Front.* 9 (4), 1163–1177. <http://dx.doi.org/10.1016/j.gsf.2018.01.006>.
- Hart, T.R., 2007. Geochronology of the hamlin and Wye Lakes Area, shebandowan greenstone belt, thunder bay district. In: Open File Report. Summary of Field Work and Other Activities 2007, vol. 6213, Ontario Geological Survey.
- Hastie, E.C.G., Kontak, D.J., Lafrance, B., 2020. Gold remobilization: Insights from gold deposits in the Archean swayze. *Econ. Geol.* 115 (2), 241–277. <http://dx.doi.org/10.5382/econgeo.4709>.
- Hastie, E.C.G., Schindler, M., Kontak, D.J., Lafrance, B., 2021. Transport and coarsening of gold nanoparticles in an orogenic deposit by dissolution-reprecipitation and oswald ripening. *Commun. Earth Environ.* 2 (1), 1–9. <http://dx.doi.org/10.1038/s43247-021-00126-6>.
- Heather, K.B., Shore, G.T., 1999. *Geology, Swayze Greenstone Belt. Tech. Rep., Ontario Geological Survey of Canada Open File 3384*, scale 1:50,000.
- Hielscher, R., Schaeben, H., 2008. A novel pole figure inversion method: specification of the MTEX algorithm. *J. Appl. Crystallogr.* 41 (6), 1024–1037. <http://dx.doi.org/10.1107/S0021889808030112>.
- Hodgson, C.J., 1989. The structure of shear-related, vein-type gold deposits: A review. *Ore Geol. Rev.* 4 (3), 231–273. [http://dx.doi.org/10.1016/0169-1368\(89\)90019-X](http://dx.doi.org/10.1016/0169-1368(89)90019-X).
- Iacopini, D., Carosi, R., Montomoli, C., Passchier, C.W., 2008. Strain analysis and vorticity of flow in the Northern Sardinian Variscan Belt: Recognition of a partitioned oblique deformation event. *Tectonophysics* 446 (1–4), 77–96. <http://dx.doi.org/10.1016/j.tecto.2007.10.002>.
- Iacopini, D., Frassi, C., Carosi, R., Montomoli, C., 2011. Biases in three-dimensional vorticity analysis using porphyroblast system: limits and application to natural examples. *Geol. Soc. Lond. Spec. Publ.* 360 (1), 301–318. <http://dx.doi.org/10.1144/SP360.17>.
- Jellicoe, K., Ciuffo, T.J., Lin, S., Wodicka, N., Wu, N., Mercier-Langevin, P., Yakymchuk, C., 2022. Genesis of the island gold deposit, ontario, Canada: Implications for gold mineralization in the Wawa subprovince of the Superior Province. *Econ. Geol.* 117 (7), 1597–1612. <http://dx.doi.org/10.5382/econgeo.4963>.
- Jessup, M.J., Law, R.D., Frassi, C., 2007. The rigid grain net (RGN): An alternative method for estimating mean kinematic vorticity number (Wm). *J. Struct. Geol.* 29 (3), 411–421. <http://dx.doi.org/10.1016/j.jsg.2006.11.003>.
- Johnson, S.E., Lenferink, H.J., Marsh, J.H., Price, N.A., Koons, P.O., West, D.P., 2009a. Kinematic vorticity analysis and evolving strength of mylonitic shear zones: New data and numerical results. *Geology* 37 (12), 1075–1078. <http://dx.doi.org/10.1130/g30227a.1>.
- Johnson, S.E., Lenferink, H.J., Price, N.A., Marsh, J.H., Koons, P.O., West, D.P., Beane, R., 2009b. Clast-based kinematic vorticity gauges: The effects of slip at matrix/clast interfaces. *J. Struct. Geol.* 31 (11), 1322–1339. <http://dx.doi.org/10.1016/j.jsg.2009.07.008>.
- Kar, E., Sarkar, D., Ghosh, P., 2024. Interpretation of geometry of greenstone belts and nature of fluid pathways for gold deposits using strain and vorticity analyses of shear zone – insights from Ramagiri-Penakacherla transcratonic shear zone system. *Geosci. J.* 28 (6), 845–860. <http://dx.doi.org/10.1007/s12303-024-0035-z>.
- Kasseem, O.M.K., Abd El Rahim, S.H., El Nashar, E.S.R., AL Kahtany, K.M., 2016. Application of kinematic vorticity and gold mineralization for the wall rock alterations of shear zone at Dungash gold mining, Central Eastern Desert, Egypt. *Geol. Ore Deposits* 58 (6), 499–515. <http://dx.doi.org/10.1134/S107501516060052>.
- Kerrick, R., Cassidy, K.F., 1994. Temporal relationships of lode gold mineralization to accretion, magmatism, metamorphism and deformation — Archean to present: A review. *Ore Geol. Rev.* 9 (4), 263–310. [http://dx.doi.org/10.1016/0169-1368\(94\)90019-9](http://dx.doi.org/10.1016/0169-1368(94)90019-9).
- Kerrick, R., Wyman, D., 1990. Geodynamic setting of mesothermal gold deposits: An association with accretionary tectonic regimes. *Geology* 18 (9), 882. [http://dx.doi.org/10.1130/0091-7613\(1990\)018<0882:GSOMGD>2.3.CO;2](http://dx.doi.org/10.1130/0091-7613(1990)018<0882:GSOMGD>2.3.CO;2).
- Kim, Y.-S., Peacock, D.C.P., Sanderson, D.J., 2004. Fault damage zones. *J. Struct. Geol.* 26 (3), 503–517. <http://dx.doi.org/10.1016/j.jsg.2003.08.002>.
- Kolb, J., 2008. The role of fluids in partitioning brittle deformation and ductile creep in auriferous shear zones between 500 and 700°C. *Tectonophysics* 446 (1–4), 1–15. <http://dx.doi.org/10.1016/j.tecto.2007.10.001>.
- Kruckenberg, S.C., Michels, Z.D., Parsons, M.M., 2019. From intracrystalline distortion to plate motion: Unifying structural, kinematic, and textural analysis in heterogeneous shear zones through crystallographic orientation-dispersion methods. *Geosphere* 15 (2), 357–381. <http://dx.doi.org/10.1130/GES01585.1>.
- Lafrance, B., DeWolfe, J.C., Stott, G.M., 2004. A structural reappraisal of the Beardmore-Geraldton Belt at the southern boundary of the Wabigoon subprovince, Ontario, and implications for gold mineralization. *Can. J. Earth Sci.* 41 (2), 217–235. <http://dx.doi.org/10.1139/e03-090>.
- Larson, K.P., Godin, L., 2009. Kinematics of the Greater Himalayan sequence, Dhaulagiri Himal: implications for the structural framework of central Nepal. *J. Geol. Soc.* 166 (1), 25–43. <http://dx.doi.org/10.1144/0016-76492007-180>.
- Law, R.D., Searle, M.P., Simpson, R.L., 2004. Strain, deformation temperatures and vorticity of flow at the top of the Greater Himalayan Slab, Everest Massif, Tibet. *J. Geol. Soc.* 161 (2), 305–320. <http://dx.doi.org/10.1144/0016-764903-047>.
- Leclair, A.D., Ernst, R.E., Hattori, K., 1993. Crustal-scale auriferous shear zones in the central superior province, Canada. *Geology* 21 (5), 399. [http://dx.doi.org/10.1130/0091-7613\(1993\)021<0399:CSASZI>2.3.CO;2](http://dx.doi.org/10.1130/0091-7613(1993)021<0399:CSASZI>2.3.CO;2).
- Lee, Y.-J., Wiltschko, D.V., 2000. Fault controlled sequential vein dilation: competition between slip and precipitation rates in the Austin Chalk, Texas. *J. Struct. Geol.* 22 (9), 1247–1260. [http://dx.doi.org/10.1016/s0191-8141\(00\)00045-6](http://dx.doi.org/10.1016/s0191-8141(00)00045-6).
- Lin, S., 2001. Stratigraphic and structural setting of the hemlo gold deposit, ontario, Canada. *Econ. Geol.* 96 (3), 477–507. <http://dx.doi.org/10.2113/gsecongeo.96.3.477>.
- Lin, S., Corfu, F., 2002. Structural setting and geochronology of auriferous quartz veins at the high rock island gold deposit, Northwestern Superior Province, Manitoba, Canada. *Econ. Geol.* 97 (1), 43–57. <http://dx.doi.org/10.2113/gsecongeo.97.1.43>.

- Lisle, R.J., 1985. The use of the orientation tensor for the description and statistical testing of fabrics. *J. Struct. Geol.* 7 (1), 115–117. [http://dx.doi.org/10.1016/0191-8141\(85\)90119-1](http://dx.doi.org/10.1016/0191-8141(85)90119-1).
- Lisle, R.J., 1989. The statistical analysis of orthogonal orientation data. *J. Geol.* 97 (3), 360–364. <http://dx.doi.org/10.1086/629309>.
- Lodge, R.W.D., Gibson, H.L., Stott, G.M., Hudak, G.J., Jirsa, M.A., Hamilton, M.A., 2013. New U-Pb geochronology from Timiskaming-type assemblages in the Shebandowan and vermilion greenstone belts, Wawa subprovince, Superior Craton: Implications for the Neoproterozoic development of the southwestern Superior Province. *Precambrian Res.* 235, 264–277. <http://dx.doi.org/10.1016/j.precamres.2013.06.011>.
- Mardia, K.V., Jupp, P.E.J., 2000. Directional statistics. In: Mardia, K.V., Jupp, P.E.J. (Eds.), In: Wiley Series in Probability and Statistics, John Wiley & Sons, Inc., Hoboken, NJ, USA, pp. 1–10. <http://dx.doi.org/10.1002/0471667196.ess7086.pub2>.
- Markey, R., Stein, H.J., Hannah, J.L., Zimmerman, A., Selby, D., Creaser, R.A., 2007. Standardizing Re-Os geochronology: A new molybdenite Reference Material (Henderson, USA) and the stoichiometry of Os salts. *Chem. Geol.* 244 (1–2), 74–87. <http://dx.doi.org/10.1016/j.chemgeo.2007.06.002>.
- McKinstry, H.E., 1948. *Mining Geology*. Prentice-Hall Inc., New York.
- McNab, R.R., Brugger, J., Voisey, C.R., Tomkins, A.G., 2024. Coprecipitation of amorphous silica and gold nanoparticles contributes to gold hyperenrichment. *Geology* 52 (10), 737–741. <http://dx.doi.org/10.1130/g52138.1>.
- Means, W.D., Hobbs, B.E., Lister, G.S., Williams, P.F., 1980. Vorticity and non-coaxiality in progressive deformations. *J. Struct. Geol.* 2 (3), 371–378. [http://dx.doi.org/10.1016/0191-8141\(80\)90024-3](http://dx.doi.org/10.1016/0191-8141(80)90024-3).
- Melo-Gómez, J., Hastie, E., Gibson, H., Tait, K., Petrus, J., 2025. Minor and trace element chemistry of gold: Controls and implications for gold deposits within the Superior Province, Canada. (2), pp. 307–333. <http://dx.doi.org/10.5382/econgeo.5148>.
- Michels, Z.D., Kruckenberg, S.C., Davis, J.R., Tikoff, B., 2015. Determining vorticity axes from grain-scale dispersion of crystallographic orientations. *Geology* 43 (9), 803–806. <http://dx.doi.org/10.1130/G36868.1>.
- Micklethwaite, S., Cox, S.F., 2006. Progressive fault triggering and fluid flow in aftershock domains: Examples from mineralized Archaean fault systems. *Earth Planet. Sci. Lett.* 250 (1–2), 318–330. <http://dx.doi.org/10.1016/j.epsl.2006.07.050>.
- Morphet, W.J., Symanzik, J., 2010. The circular dataimage, a graph for high-resolution circular-spatial data. *Int. J. Digit. Earth* 3 (1), 47–71. <http://dx.doi.org/10.1080/17538940903277657>.
- Muir, T.L., 2003. Structural evolution of the Hemlo greenstone belt in the vicinity of the world-class Hemlo gold deposit. *Can. J. Earth Sci.* 40 (3), 395–430. <http://dx.doi.org/10.1139/e03-004>.
- Müller, D., Kwan, K., Groves, D.I., 2021. Geophysical implications for the exploration of concealed orogenic gold deposits: A case study in the Sandy Lake and Favourable Lake Archean greenstone belts, Superior Province, Ontario, Canada. *Ore Geol. Rev.* 128, 103892. <http://dx.doi.org/10.1016/j.oregeorev.2020.103892>.
- Newhouse, W.H., 1942. Ore deposits as Related to Structural Features. Princeton, New Jersey, USA, p. 280.
- Ontario Geological Survey, 2011. 1:250 000 Scale Bedrock Geology of Ontario. Data 126 - Revision 1. Tech. rep., Ontario Geological Survey.
- Ontario Geological Survey, 2024. Ontario mineral inventory.
- Osmani, I.A., 1993. Geology and mineral potential of Moss Township, District of Thunder Bay. Tech. Rep. 5865, Ontario Geological Survey, Open File Report.
- Osmani, I.A., 1997. Geology and Mineral Potential, Greenwater Lake Area, West-Central Shebandowan Greenstone Belt. Tech. Rep. 296, Ontario Geological Survey, Report.
- Pan, Y., Fleet, E., Michael, Heaman, L., 1998. Thermo-tectonic evolution of an archean accretionary complex: U-Pb geochronological constraints on granulites from the Quetico subprovince, Ontario, Canada. *Precambrian Res.* 92 (2), 117–128. [http://dx.doi.org/10.1016/S0301-9268\(98\)00070-9](http://dx.doi.org/10.1016/S0301-9268(98)00070-9).
- Pan, Y., Fleet, E., Williams, H.R., 1994. Granulite-facies metamorphism in the Quetico Subprovince, north of Manitouwadge, Ontario. *Can. J. Earth Sci.* 31 (9), 1427–1439. <http://dx.doi.org/10.1139/e94-126>.
- Passchier, C.W., 1987. Stable positions of rigid objects in non-coaxial flow—a study in vorticity analysis. *J. Struct. Geol.* 9 (5–6), 679–690. [http://dx.doi.org/10.1016/0191-8141\(87\)90152-0](http://dx.doi.org/10.1016/0191-8141(87)90152-0).
- Percival, J.A., 1989. A regional perspective of the Quetico metasedimentary belt, Superior Province, Canada. In: *J. Earth Sci. Can. J. Earth Sci.* 26, 677–693.
- Percival, J., Skulski, T., Sanborn-Barrie, M., Stott, G., Leclair, A., Corkery, T., Boily, M., 2012. Geology and tectonic evolution of the Superior Province, Canada. In: Percival, J.A., Cook, F.A., Clowes, R.M. (Eds.), *Tectonic Styles in Canada: The Lithoprobe Perspective*. In: Special Paper, (49), Geological Survey of Canada.
- Percival, J.A., Williams, H.R., 1989. Late Archean Quetico accretionary complex, Superior province, Canada. *Geology* 17, 23–25.
- Petrella, L., Thébaud, N., Fougerouse, D., Evans, K., Quadir, Z., Laflamme, C., 2020. Colloidal gold transport: a key to high-grade gold mineralization? *Miner. Deposita* 55 (7), 1247–1254. <http://dx.doi.org/10.1007/s00126-020-00965-x>.
- Phillips, G.N., Powell, R., 2009. Formation of gold deposits: Review and evaluation of the continuum model. *Earth-Sci. Rev.* 94 (1–4), 1–21. <http://dx.doi.org/10.1016/j.earscirev.2009.02.002>.
- Pitcairn, I.K., Teagle, D.A.H., Craw, D., Olivo, G.R., Kerrich, R., Brewer, T.S., 2006. Sources of metals and fluids in orogenic gold deposits: Insights from the Otago and Alpine schists, New Zealand. *Econ. Geol.* 101 (8), 1525–1546. <http://dx.doi.org/10.2113/gsecongeo.101.8.1525>.
- Poulsen, K.H., Robert, F., Card, K.D., 1992. Transpressive tectonics and the Archean gold deposits of Superior Province, Canadian Shield. In: Bartholomew, M.J., Hyndman, D.W., Mogk, D.W., Mason, R. (Eds.), In: *Basement Tectonics 8: Proceedings of the International Conferences on Basement Tectonics*, vol. 2, Springer Netherlands, pp. 615–623. http://dx.doi.org/10.1007/978-94-011-1614-5_43.
- Rauchenstein-Martinek, K., Wagner, T., Wölle, M., Heinrich, C.A., 2014. Gold concentrations in metamorphic fluids: A LA-ICPMS study of fluid inclusions from the Alpine orogenic belt. *Chem. Geol.* 385, 70–83. <http://dx.doi.org/10.1016/j.chemgeo.2014.07.018>.
- Rispoli, R., 1981. Stress fields about strike-slip faults inferred from stylolites and tension gashes. *Tectonophysics* 75 (3–4), T29–T36. [http://dx.doi.org/10.1016/0040-1951\(81\)90274-2](http://dx.doi.org/10.1016/0040-1951(81)90274-2).
- Rogers, M.C., Berger, B., 1994. *Geology of Adrian, Marks, Sackville, Aldina and Duckworth Townships, District of Thunder Bay*. Tech. Rep., Ontario Geological Survey, p. 102.
- Romer, R.L., Kroner, U., 2018. Paleozoic gold in the Appalachians and Variscides. *Ore Geol. Rev.* 92, 475–505. <http://dx.doi.org/10.1016/j.oregeorev.2017.11.021>.
- Sawyer, E.W., 1983. The structural history of a part of the Archean Quetico Metasedimentary Belt, Superior Province, Canada. *Precambrian Res.* 22 (3–4), 271–294. [http://dx.doi.org/10.1016/0301-9268\(83\)90052-9](http://dx.doi.org/10.1016/0301-9268(83)90052-9).
- Sawyer, E.W., Barnes, S.J., 1988. Temporal and compositional differences between subsolidus and anatetic migmatite leucosomes from the Quetico metasedimentary belt, Canada. *J. Metamorph. Geol.* 6 (4), 437–450. <http://dx.doi.org/10.1111/j.1525-1314.1988.tb00432.x>.
- Schaeben, H., Hielscher, R., Fundenberger, J.-J., Potts, D., Prestin, J., 2007. Orientation density function-controlled pole probability density function measurements: automated adaptive control of texture goniometers. *J. Appl. Crystallogr.* 40 (3), 570–579. <http://dx.doi.org/10.1107/S0021889807019711>.
- Scheidegger, A.E., 1964. The tectonic stress and tectonic motion direction in Europe and Western Asia as calculated from earthquake fault plane solutions. *Bull. Seismol. Soc. Am.* 54 (5A), 1519–1528. <http://dx.doi.org/10.1785/bssa05405a1519>.
- Schneiders, B.R., Gupta, R.J., 1985. *Property Visits and Reports of the Atikokan Economic Geologist, 1979–1983*. Atikokan Geological Survey. Tech. Rep., (5539), Atikokan Geological Survey, Ontario Geological Survey. Open File Report.
- Scoates, J.S., Friedman, R.M., 2008. Precise age of the platiniferous Merensky Reef, Bushveld Complex, South Africa, by the U-Pb zircon chemical abrasion ID-TIMS technique. *Econ. Geol.* 103 (3), 465–471. <http://dx.doi.org/10.2113/gsecongeo.103.3.465>.
- Selby, D., Creaser, R.A., 2004. Macroscale NTIMS and microscale LA-MC-ICP-MS Re-Os isotopic analysis of molybdenite: Testing spatial restrictions for reliable Re-Os age determinations, and implications for the decoupling of Re and Os within molybdenite. *Geochim. Cosmochim. Acta* 68 (19), 3897–3908. <http://dx.doi.org/10.1016/j.gca.2004.03.022>.
- Seward, T.M., 1973. Thio complexes of gold and the transport of gold in hydrothermal ore solutions. *Geochim. Cosmochim. Acta* 37 (3), 379–399. [http://dx.doi.org/10.1016/0016-7037\(73\)90207-X](http://dx.doi.org/10.1016/0016-7037(73)90207-X).
- Seward, T.M., Williams-Jones, A.E., Migdisov, A.A., 2014. The chemistry of metal transport and deposition by ore-forming hydrothermal fluids, second ed. In: *Treatise on Geochemistry*, vol. 13, Elsevier Ltd., pp. 29–57. <http://dx.doi.org/10.1016/B978-0-08-095975-7.01102-5>.
- Shenberger, D.M., Barnes, H.L., 1989. Solubility of gold in aqueous sulfide solutions from 150 to 350°C. *Geochim. Cosmochim. Acta* 53 (2), 269–278. [http://dx.doi.org/10.1016/0016-7037\(89\)90379-7](http://dx.doi.org/10.1016/0016-7037(89)90379-7).
- Sibson, R.H., 1986. Brecciation processes in fault zones: Inferences from earthquake rupturing. *Pure Appl. Geophys.* 124 (1–2), 159–175. <http://dx.doi.org/10.1007/bf00875724>.
- Sibson, R.H., Moore, J.M.M., Rankin, A.H., 1975. Seismic pumping—a hydrothermal fluid transport mechanism. *J. Geol. Soc.* 131 (6), 653–659. <http://dx.doi.org/10.1144/gsjgs.131.6.0653>.
- Sibson, R.H., Robert, F., Poulsen, K.H., 1988. High-angle reverse faults, fluid-pressure cycling, and mesothermal gold-quartz deposits. *Geology* 16 (6), 551. [http://dx.doi.org/10.1130/0091-7613\(1988\)016<0551:harfp>2.3.co;2](http://dx.doi.org/10.1130/0091-7613(1988)016<0551:harfp>2.3.co;2).
- Sillitoe, R.H., 2020. Gold deposit types: An overview. In: *Geology of the World's Major Gold Deposits and Provinces*. Society of Economic Geologists, pp. 1–28. <http://dx.doi.org/10.5382/SP.23.01>, chap. 1.
- Simpson, C., De Paor, D.G., 1993. Strain and kinematic analysis in general shear zones. *J. Struct. Geol.* 15 (1), 1–20. [http://dx.doi.org/10.1016/0191-8141\(93\)90075-L](http://dx.doi.org/10.1016/0191-8141(93)90075-L).
- Simpson, C., De Paor, D.G., 1997. Practical analysis of general shear zones using the porphyroblast hyperbolic distribution method: An example from the Scandinavian Caledonides. In: Sengupta, S. (Ed.), *Evolution of Geological Structures in Micro- To Macro-Scales*. Springer Netherlands, Dordrecht, pp. 169–184. http://dx.doi.org/10.1007/978-94-011-5870-1_10.
- Smoliar, M.I., Walker, R.J., Morgan, J.W., 1996. Re-Os ages of group IIA, IIIA, IVA, and IVB iron meteorites. *Science* 271 (5252), 1099–1102. <http://dx.doi.org/10.1126/science.271.5252.1099>.

- Stacey, J.S., Kramers, J.D., 1975. Approximation of terrestrial lead isotope evolution by a two-stage model. *Earth Planet. Sci. Lett.* 26 (2), 207–221. [http://dx.doi.org/10.1016/0012-821X\(75\)90088-6](http://dx.doi.org/10.1016/0012-821X(75)90088-6).
- Stahr, D.W., Law, R.D., 2011. Effect of finite strain on clast-based vorticity gauges. *J. Struct. Geol.* 33 (7), 1178–1192. <http://dx.doi.org/10.1016/j.jsg.2011.05.002>.
- Stephan, T., 2024. tectonicr: Analyzing the orientation of maximum horizontal stress. <http://dx.doi.org/10.32614/CRAN.package.tectonicr>.
- Stephan, T., 2025. Structural data for article Stephan et al. “Going with the flow — changes of vorticity control gold enrichment in Archean shear zones (Shebandowan Greenstone Belt, Superior Province, Canada)”. <http://dx.doi.org/10.17605/OSF.IO/C4EY9>.
- Stephan, T., Enkelmann, E., Kroner, U., 2023. Analyzing the horizontal orientation of the crustal stress adjacent to plate boundaries. *Sci. Rep.* 13 (1), 15590. <http://dx.doi.org/10.1038/s41598-023-42433-2>.
- Thurston, P.C., Ayer, J.A., Goutier, J., Hamilton, M.A., 2008. Depositional gaps in abitibi greenstone belt stratigraphy: A key to exploration for syngenetic mineralization. *Econ. Geol.* 103, 1097–1134.
- Tikoff, B., Teyssier, C., 1994. Strain modeling of displacement-field partitioning in transpressional orogens. *J. Struct. Geol.* 16 (11), 1575–1588. [http://dx.doi.org/10.1016/0191-8141\(94\)90034-5](http://dx.doi.org/10.1016/0191-8141(94)90034-5).
- Tomkins, A.G., Pattison, D.R.M., Frost, B.R., 2007. On the initiation of metamorphic sulfide anatexis. *J. Petrol.* 48 (3), 511–535. <http://dx.doi.org/10.1093/petrology/egl070>.
- Tomkins, A.G., Pattison, D.R.M., Zaleski, E., 2004. The hemlo gold deposit, ontario: An example of melting and mobilization of a precious metal-sulfosalt assemblage during amphibolite facies metamorphism and deformation. *Econ. Geol.* 99 (6), 1063–1084. <http://dx.doi.org/10.2113/gsecongeo.99.6.1063>.
- Tooth, B., Ciobanu, C.L., Green, L., O'Neill, B., Brugger, J., 2011. Bi-melt formation and gold scavenging from hydrothermal fluids: An experimental study. *Geochim. Cosmochim. Acta* 75 (19), 5423–5443. <http://dx.doi.org/10.1016/j.gca.2011.07.020>.
- Tóth, Z., Lafrance, B., Dubé, B., 2023. Oblique lateral extrusion during dextral transpression along the Beardmore-Geraldton belt, Canada. *J. Struct. Geol.* 169, 104834. <http://dx.doi.org/10.1016/j.jsg.2023.104834>.
- Truesdell, C., 1953. Two measures of vorticity. *J. Ration. Mech. Anal.* 2, 173–217.
- Voisey, C.R., Hunter, N.J.R., Tomkins, A.G., Brugger, J., Liu, W., Liu, Y., Luzin, V., 2024. Gold nugget formation from earthquake-induced piezoelectricity in quartz. *Nat. Geosci.* 17 (9), 920–925. <http://dx.doi.org/10.1038/s41561-024-01514-1>.
- Voisey, C.R., Willis, D., Tomkins, A.G., Wilson, C.J.L., Micklethwaite, S., Salvemini, F., Bougoure, J., Rickard, W.D.A., 2020. Aseismic refinement of orogenic gold systems. *Econ. Geol.* 115 (1), 33–50. <http://dx.doi.org/10.5382/econgeo.4692>.
- Vollmer, F.W., 1990. An application of eigenvalue methods to structural domain analysis. *Geol. Soc. Am. Bull.* 102, 786–791.
- Vollmer, F.W., 2020. Representing progressive fabric paths on a triangular plot using a fabric density index and crystal axes eigenvector barycenters. In: Geological Society of America Abstracts with Programs, vol. 52, (6), Geological Society of America, Online, <http://dx.doi.org/10.1130/abs/2020am-358862>.
- Weatherley, D.K., Henley, R.W., 2013. Flash vaporization during earthquakes evidenced by gold deposits. *Nat. Geosci.* 6 (4), 294–298. <http://dx.doi.org/10.1038/ngeo1759>.
- Williams, H.R., Stott, G.M., Heather, K.B., Muir, T.L., Sage, R.P., 1991. Wawa subprovince. In: *Geology of Ontario*, vol. 4, (1), Ontario Geological Survey, pp. 484–539.
- Williams-Jones, A.E., Bowell, R.J., Migdisov, A.A., 2009. Gold in solution. *Elements* 5 (5), 281–287. <http://dx.doi.org/10.2113/gselements.5.5.281>.
- Wise, S.A., Watters, R.L., 2011. Reference Material 8599 Henderson Molybdenite. Tech. Rep. 30, National Institute of Standards and Technology, Report of Investigation.
- Wood, P.C., Burrows, D.R., Thomas, A.V., Spooner, E.T.C., 1986. The Holliger-McIntyre Au-quartz vein system: Geological characteristics, gold occurrence, fluid properties and light stable isotope geochemistry. *Proc. Gold* 86, 53–80.
- Woodcock, N.H., 1977. Specification of fabric shapes using an eigenvalue method. *GSA Bull.* 88 (9), 1231–1236. [http://dx.doi.org/10.1130/0016-7606\(1977\)88<1231:sofsua>2.0.co;2](http://dx.doi.org/10.1130/0016-7606(1977)88<1231:sofsua>2.0.co;2).
- Xypolias, P., 2010. Vorticity analysis in shear zones: A review of methods and applications. *J. Struct. Geol.* 32 (12), 2072–2092. <http://dx.doi.org/10.1016/j.jsg.2010.08.009>.
- Yardley, B., 1996. Earthquakes with gold linings. *Nature* 382 (6588), 210–211. <http://dx.doi.org/10.1038/382210a0>.
- Zaleski, E., van Breemen, O., Peterson, V.L., 1999. Geological evolution of the Manitouwadge greenstone belt and Wawa — Quetico subprovince boundary, Superior Province, Ontario, constrained by U-Pb zircon dates of supracrustal and plutonic rocks. *Can. J. Earth Sci.* 36 (6), 945–966. <http://dx.doi.org/10.1139/e99-016>.
- Zammit, K., Perrotty, S., Frieman, B.M., Marsh, J.H., Holt, K.A., 2022. Structural and geochronological constraints on orogenic gold mineralization in the western Wabigoon subprovince, Canada. *Can. J. Earth Sci.* 59 (5), 278–299. <http://dx.doi.org/10.1139/cjes-2021-0042>.